Using Thermochronology to Understand Orogenic Erosion

Peter W. Reiners and Mark T. Brandon

Department of Geology and Geophysics, Kline Geology Laboratory, Yale University, New Haven, Connecticut 06511; email: peter.reiners@yale.edu, mark.brandon@yale.edu

Annu. Rev. Earth Planet. Sci. 2006. 34:419–66

First published online as a Review in Advance on January 16, 2006

The *Annual Review of Earth and Planetary Science* is online at earth.annualreviews.org

doi: 10.1146/annurev.earth.34.031405.125202

0084-6597/06/0530-0419$20.00

Key Words

geochronology, exhumation, orogeny, geomorphology, tectonics

Abstract

Erosion of orogenic mountain ranges exhumes deeply buried rocks and controls weathering, climate, and sediment production and transport at a variety of scales. Erosion also affects the topographic form and kinematics of orogens, and it may provide dynamic feedbacks between climate and tectonics by spatially focused erosion and rock uplift. Thermochronology measures the timing and rates at which rocks approach the surface and cool as a result of exhumation. Relatively well-understood noble gas and fission-track thermochronometric systems have closure temperatures ranging from ~60 to ~550°C, making them sensitive to exhumation through crustal depths of about one to tens of kilometers. Thus, thermochronology can constrain erosion rates and their spatial-temporal variations on timescales of $\sim 10^5$–10^7 years, commensurate with orogenic growth and decay cycles and possible climate-tectonic feedback response times. Useful methods for estimating erosion rates include inverting ages for erosion rates using crustal thermal models, vertical transects, and detrital approaches. Spatial-temporal patterns of thermochronometrically determined erosion rates help constrain flow of material through orogenic wedges, orogenic growth and decay cycles, paleorelief, and relationships with structural, geomorphic, or climatic features.

INTRODUCTION

Rock uplift/surface uplift: vertical motion of rock or a portion of the Earth near or at the surface, relative to a datum, such as sea level

Erosion: the surficial removal of mass at a point in the landscape by both mechanical and chemical processes

Denudation: the removal of rock or soil by tectonic and/or surficial processes at a specified point at or under Earth's surface. Denudation can be tectonic (normal faulting or ductile thinning) or erosional

Exhumation: the unroofing history or path of a rock toward Earth's surface, as a result of a denudational process. Exhumation is also either tectonic or erosional

Orogens (mountain ranges formed by tectonic processes) control the patterns and scales of a wide variety of phenomena, including weathering, erosion, climate, hydrology, sediment transport and deposition, biotic distributions, and natural resources and hazards. The configuration and architecture of orogens also provide clues to the dynamics of mantle convection and the movement of tectonic plates, and the exhumed rocks within them provide samples of the deep crust and upper mantle. Understanding the growth and decay of orogens thus provides a basic framework for understanding many other natural processes and their interactions.

Three interrelated processes are commonly used to describe the tectonic geomorphology of orogens: rock uplift, surface uplift, and erosion. As clarified by England & Molnar (1990), rock and surface uplift describe the vertical motion of rock or a portion of Earth's surface, respectively, relative to a datum, such as sea level, that is suitably fixed. Erosion is the surficial removal of mass at a point in the landscape by both mechanical and chemical processes. It follows, then, that the difference between rock uplift and surface uplift is erosion. For example, surface uplift, which contributes to mountainous topography, only occurs when erosion is slower than rock uplift. Erosion is one type of the broader process of denudation, which, following Ring et al. (1999a), is the removal of rock or soil by tectonic and/or surficial processes at a specified point at or under Earth's surface. The other types of denudation are tectonic: normal faulting and ductile thinning. Incidentally, it is important to note that crustal thickening by ductile or brittle strain (e.g., thrusting) causes burial, not denudation, although thickening can produce high topography, which may result in erosion. Another term that is frequently used in studying orogenic evolution is exhumation, which Ring et al. (1999a) defined as the unroofing history of a rock, as caused by tectonic and/or surficial processes. Thus, exhumation is the history of or path taken by a particular rock toward the surface, as a result of a denudational process.

Erosion plays a critical role in orogenic evolution in several ways. First, it often follows rock and surface uplift in space and time, providing an indirect constraint on the spatial and temporal patterns of uplift in a landscape, which may be otherwise difficult to observe directly. More generally, erosion is a dynamic link between tectonic uplift and many other processes, including chemical weathering and long-term climate change, and sediment production, routing, and deposition. Most immediately, however, erosion directly influences not only topographic decay, but also growth of an orogen, by modulating the pattern and rates of surface uplift. Because erosion is also related to climate (e.g., precipitation), it provides an important feedback between climate and tectonics. Thus, interpreting how climate affects orogeny requires understanding erosion.

Rates of erosion over short timescales (1–10 years) can be estimated by sediment loads carried by rivers, but this can be difficult to extrapolate to longer timescales, largely because of the influence of large, infrequent erosional events, such as landslides (Hovius et al. 1997, Kirchner et al. 2001, Burbank 2002). Cosmogenic nuclide measurements made on fluvial sediment or in-situ materials can provide erosion rate estimates over timescales of typically 10^3–10^4 years, capturing rates closer to

those over longer terms, and integrating an effective erosion rate signal through several meters depth (Brown et al. 1995, Bierman & Steig 1996, Granger et al. 1996, Kirchner et al. 2001, Riebe et al. 2003). However, many important geologic processes and feedbacks operate on timescales commensurate with large-scale rock deformation, at roughly 10^5–10^7 year scales, requiring understanding of the spatial-temporal patterns of erosion on longer timescales. Erosion rates in active and decaying mountain ranges are typically 0.05–10 km Myr^{-1}, with total erosion reaching depths of about 5–30 km. These depths are too great for cosmogenic approaches, and, in many cases, total erosion depths are too shallow to estimate using thermobarometric-geochronologic constraints. Many radioisotopic thermochronometers, however, are well suited to this task because they are sensitive to temperature changes between about 60–550°C, corresponding to crustal depths of about 2–10 km.

In this chapter, we review general aspects of the use of thermochronology for the study of orogenic erosion, beginning with the fundamental bases of thermochronometric systems commonly used for this purpose, with an emphasis on K/Ar (and $^{40}Ar/^{39}Ar$), (U-Th)/He, and fission-track methods. We then review some basic concepts of the thermal structure of the shallow crust and how it is influenced by erosion and topography, and how these factors can be accounted for in the interpretation of thermochronologic data. We then describe several important techniques used in both active and decaying orogens for interpreting the spatial and temporal patterns of erosion, and provide examples illustrating the insights these approaches provide.

THERMOCHRONOLOGY

The (U-Th)/He, fission-track (FT), and $^{40}Ar/^{39}Ar$ dating methods are the three main thermochronologic methods in use today that allow constraints on thermal histories at temperatures below approximately 300–550°C. All are based on the production, by nuclear decay, of an isotope or radiation damage and the thermally controlled retention of these decay products. Radioisotopic production decreases exponentially with time but is predictable and otherwise steady, which gives the thermochronometer the ability to keep time. The thermal sensitivity of these radioisotopic clocks means that they provide information about the cooling history of rock, rather than the crystallization ages of its minerals (although in some cases they do record crystallization ages as well). We refer to these ages as cooling ages in that they tell us the duration of time that the dated mineral has been cool enough to retain the decay product of interest. We provide a brief summary here, as needed to understand the thermal behavior of these dating methods. Interested readers are referred to Farley (2002), Wagner & van den Haute (1992), McDougall & Harrison (1999), and Hodges (2003) for more detailed accounts.

We use several idealized model calculations to illustrate the thermal behavior of the thermochronometers. All of the examples below were calculated using three programs, CLOSURE, AGE2EDOT, and RESPTIME (Brandon 2005, as summarized in Ehlers et al. 2005), which are available by following the Supplemental Material link from the Annual Reviews home page at **http://www.annualreviews.org.**

Interested readers will find these programs useful for exploring thermochronometers or conditions not considered here.

RSE: relative standard error, which is equal to the standard error divided by the mean. The standard error is also called the standard deviation of the mean, and it provides an estimate of the uncertainty for the mean age

FT: fission track

(U-Th)/He Method

The (U-Th)/He method (He dating) is based on the accumulation of ^{4}He produced by the decay of the parent isotopes ^{238}U, ^{235}U, ^{232}Th, and ^{147}Sm. Radiogenic ^{4}He diffuses out of the mineral at a rate determined by the temperature and the He diffusivity of the mineral. Thus, the concentrations of ^{4}He and the parent isotopes can be used to calculate a He cooling age. Measurements are typically made using a two-stage analytical procedure involving degassing of the crystal by heating and gas-source mass spectrometry to measure ^{4}He, followed by inductively-coupled plasma mass spectrometry on the same crystal to measure U and Th (and, in some cases, Sm). Grain ages typically have a relative standard error (RSE) of approximately 3% to 5%, as determined by replicate measurements.

Fission-Track Method

The fission-track (FT) method utilizes the damage produced by fission decay of ^{238}U. Fission causes ^{238}U to split into two atomic fragments, which produces ionization damage along their repulsive paths. Fresh FTs have a total length of ~11 μm in zircon and ~16 μm in apatite. The track is thought to be a region of high defect density, not because of collision by the fission fragments, but rather because of changes in charge along the flight paths of the fission fragments. This ionization damage causes widespread dislocation of atoms from their stable lattice positions along the fission track (Fleischer et al. 1975). This interpretation explains why tracks are only found in nonconductive minerals. Thermally activated diffusion allows the defects to migrate and the damage to anneal. Thus, temperatures must remain low for FTs to be retained on a geologic timescale. The defects are known to have a range of activation energies for annealing (Ketcham et al. 1999), which accounts for the more complex retention behavior of FTs relative to that for He and Ar retention, which are well described by simple diffusion of an inert noble gas.

FTs are measured using a high-power optical microscope. The mineral grains to be dated are mounted, polished, and then chemically etched. The tracks etch more rapidly and thus become visible for counting. The concentration of the parent isotope is determined by neutron irradiation in a nuclear reactor, which induces fission of ^{235}U. The natural ^{235}U/^{238}U ratio is fixed, so the concentration of one isotope can be used to estimate the other. A sheet of U-free mica is placed over the polished grains of the mount. Chemical etching of this mica monitor reveals the density of induced ^{235}U fission events. The induced tracks are also present in the mounted minerals, but they are not revealed given that the chemical etching of the minerals is done before the irradiation. The mica monitor and the mount are assembled with registration marks, which allows the operator to measure, in individual mineral grains, the spontaneous tracks (produced by ^{238}U fission decay over geologic time) and the induced tracks (produced by neutron irradiation). FT grain ages have a RSE of ~12% for zircon

and ~50% for apatite [median values from large compilation of detrital grain ages in Brandon (1996)]. FT ages are usually based on an average of many grain ages. In this case, the RSE for the age is typically 5% to 10%.

$^{40}Ar/^{39}Ar$ Method

The $^{40}Ar/^{39}Ar$ method (Ar dating) is based on decay of ^{40}K to radiogenic ^{40}Ar. Like He, Ar is a noble gas, and the retention of ^{40}Ar is controlled by thermally activated diffusion (although in some cases partitioning between phases can play an important role; Kelley & Wartho 2000, Baxter 2003). Argon diffusion is slower than that of He, probably owing mainly to its larger atomic radius. As a result, Ar cooling ages tend to be older than He cooling ages. Ar ages are determined by gas source mass spectrometry using a method that allows simultaneous determination of the parent ^{40}K, often in the same subcrystalline diffusion domain. This is accomplished by conversion of some fraction of ^{39}K to ^{39}Ar by neutron irradiation prior to degassing and analysis. The concentration of the parent ^{40}K can then be calculated knowing the production rate of ^{39}Ar during the neutron irradiation and the $^{40}K/^{39}K$ ratio, which is fixed for natural K. The ratio of $^{40}Ar/^{39}Ar$ is then used to calculate the Ar cooling age. The RSE for grain ages is sometimes less than 1%, but the average is ~5% (e.g., $^{40}Ar/^{39}Ar$ grain ages for detrital white micas from Brewer et al. 2005). A key advantage of conventional $^{40}Ar/^{39}Ar$ dating is that step-heating and sequential gas analysis of single samples often reveals age spectra that reveal diffusion kinetics specific to the sample. These can often be modeled as representing continuous time-temperature histories (e.g., Harrison et al. 2005). Alternatively, $^{40}Ar/^{39}Ar$ ages can be measured in subcrystalline microdomains with high spatial resolution by laser ablation methods, to determine thermal, growth, or deformational histories (e.g., Kelley et al. 1994, Kramar et al. 2001, Mulch et al. 2002).

THERMALLY ACTIVATED DIFFUSION AND PARTIAL RETENTION

There has been much study, both in the lab and in natural systems, of the thermal sensitivity of He, FT, and Ar retention and how this sensitivity can be used to estimate cooling histories. The most common approach is to use laboratory stepwise heating experiments to calibrate relationships between decay-product retention as a function of temperature and time (e.g., Fechtig & Kalbitzer 1966, Naeser & Faul 1969, Zeitler et al. 1987). These results are complemented by dating of drill samples from boreholes, where the modern thermal profile can be directly measured (e.g., Gleadow & Duddy 1981, Green et al. 1989, House et al. 2002, Stockli & Farley 2004). Exhumation by normal faulting has produced some exposed sections of continental crust. These settings have also proven useful for understanding retention behavior of thermochronometers as a function of increasing depth and temperature (Reiners et al. 2000, Stockli et al. 2000, Stockli 2005).

Although in general there is a remarkable degree of agreement among these methods, some studies have also identified important complexities in the thermal

sensitivities of the thermochronometers, mainly related to the influence of compositional effects and bulk radiation damage in the host mineral and difficulties in extrapolating laboratory studies to geologic timescales. One good way to illustrate these issues is to consider the partial retention behavior of the thermochronometer as a function of time and temperature (**Figure 1**).

Partial retention zone (PRZ): temperature or depth range where the radioisotopic decay products (e.g., ^{40}Ar, fission tracks, or ^{4}He) are only partially retained owing to thermally activated diffusion or annealing

PAZ: partial annealing zone, defined as the zone in the crust where FTs are partially retained. This term is synonymous with the more general term PRZ

Helium, Ar, and FT thermochronologists recognized early on that ages could be reset by heating, or may not even begin to accumulate decay products until cooling through a relatively low temperature (e.g., Hurley 1954, Armstrong 1966, Naeser & Faul 1969; also see summary in Reiners et al. 2005b). Because of the typically systematic relationship between temperature and depth beneath Earth's surface, this naturally leads to a useful conceptualization of how thermochronologic ages change as a function of depth. At a relatively great depth, ages are zero because temperatures are high and decay products cannot accumulate in the mineral. At some shallow depth, ages are finite, reflecting the rate of, or time since, cooling of the crustal section. Between these zones of full retention and full loss of decay products is the partial retention zone (PRZ).

The idea of a partial stability zone was first recognized in the early 1980s with the study of apatite FT ages from deep boreholes, such as the exploratory holes in the Otway Basin of SE Australia (Gleadow & Duddy 1981). Gleadow & Fitzgerald (1987) introduced the term partial annealing zone (PAZ), which is widely used today in the FT community. The Ar and He communities adopted a similar term, PRZ, in the late 1990s (Baldwin & Lister 1998, Wolf et al. 1998). We prefer this term, given that it can be applied to all thermochronometers, whereas PAZ refers specifically to the annealing of FTs. Partial retention is relatively simple to define for He and Ar dating, so we start with that topic first. We then follow with a discussion of partial retention for FT dating, with a goal to show the commonality of this concept for these different dating methods.

Laboratory diffusion experiments have demonstrated that on laboratory timescales the diffusivities of He and Ar are well fit by

$$D = D_0 \exp\left[\frac{-E_a - PV_a}{RT}\right], \quad (1)$$

where D_0 is the frequency factor ($m^2\ s^{-1}$), E_a is the activation energy ($J\ mol^{-1}$), P is pressure (Pa), V_a is the activation volume ($m^3\ mol^{-1}$), T is temperature (K), R is the gas law constant (8.3145 $J\ mol^{-1}\ K^{-1}$), and D is the diffusivity ($m^2\ s^{-1}$). The PV_a term is commonly taken as zero because most thermochronometers are retentive only at shallow depths in the crust ($<\sim$10 km), where pressures are similar to those of the laboratory diffusion studies. Lister & Baldwin (1996) noted that subduction zone settings may provide an important exception for higher-temperature thermochronometers. The low-temperature, high-pressure conditions in subduction zones can result in temperatures of 350°C at 35 km and deeper. Muscovite is able to retain Ar on geologic timescales at these temperatures, so the contribution of the PV_a term is significant. We return to this issue below.

Measured diffusion properties from **Table 1** are used to estimate the PRZ for commonly used He and Ar thermochronometers. Partial retention is usually measured

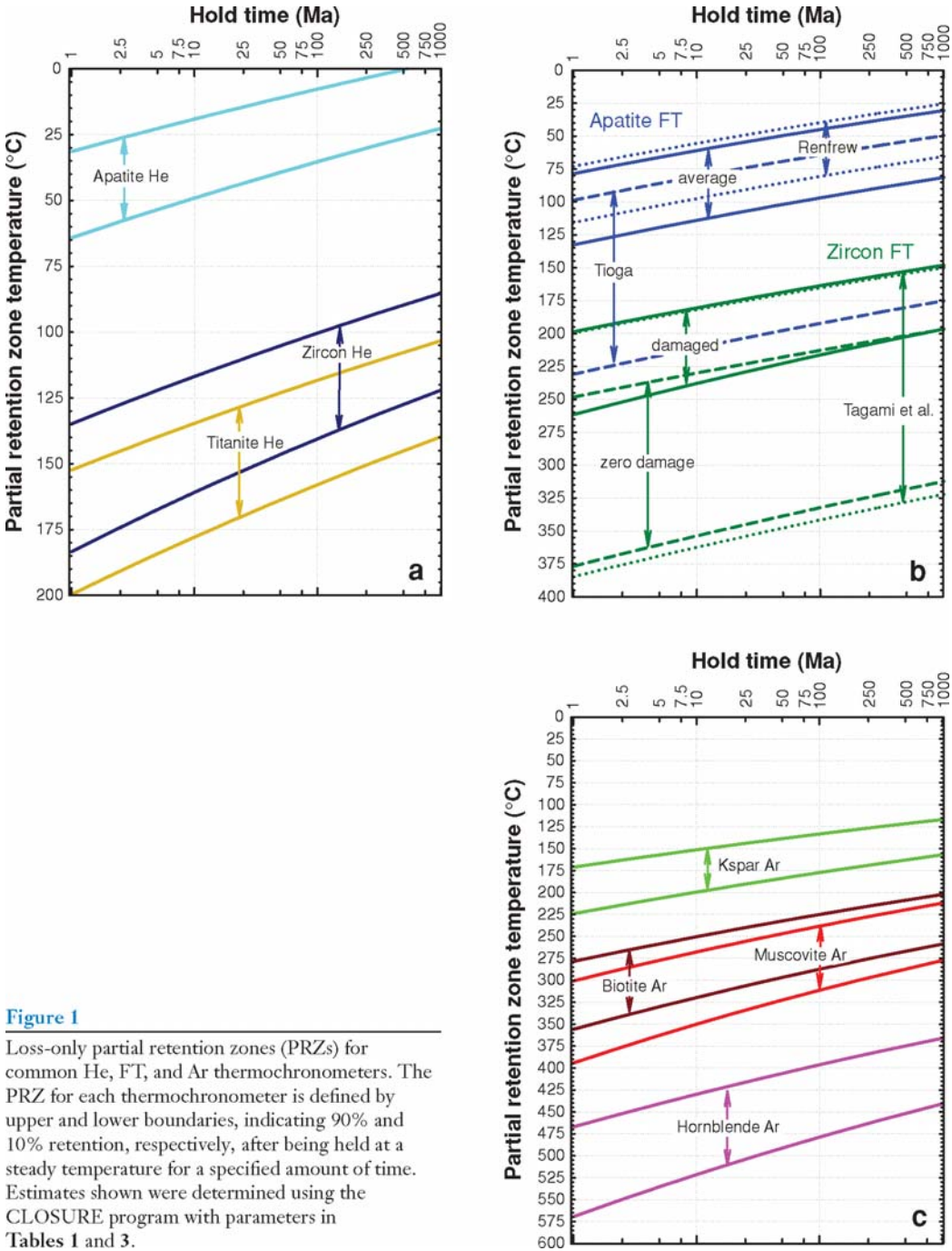

Figure 1

Loss-only partial retention zones (PRZs) for common He, FT, and Ar thermochronometers. The PRZ for each thermochronometer is defined by upper and lower boundaries, indicating 90% and 10% retention, respectively, after being held at a steady temperature for a specified amount of time. Estimates shown were determined using the CLOSURE program with parameters in **Tables 1** and **3**.

Converted to use same geometry factor (sphere) = 55
Bi: D_0 = 1.50 x 10^{-1} cm^2/s, a = 500 microns (typical cylinder radius), Ω=3300, Tc10 = 325 C
Mu (Robbins): D_0 = 7.8 x 10^{-4} cm^2/s, a = 500 microns (typical cylinder radius), Ω=17.2, Tc10 = 354 C
Mu (Hames guess): Ea = 218 kJ/mol, D_0 = 8 x 10^{-1} cm^2/s, a = 500 microns, Ω=17600, Tc10 = 362 C
Hb: D_0 = 2.40 x 10^{-2} cm^2/s, a = 80 microns (effective diffusion radius), Ω=20625, Tc10 = 501 C
Note some errors in reporting below for D0 and a for Hb.

Method (references)	(kJ mol^{-1})	D_0 (cm^2 s^{-1})	a_s^* (μm)	Ω** (s^{-1})	(C)
$^{40}Ar/^{39}Ar$ K-feldspar (orthoclase) (Foland 1994)	183	9.80 × 10^{-3}	10	5.39 × 10^5	223
$^{40}Ar/^{39}Ar$ Fe-Mg biotite (Grove & Harrison 1996)	197	7.50 × 10^{-2}	750 (500)	733	348
$^{40}Ar/^{39}Ar$ muscovite (Robbins 1972, Hames & Bowring 1994)	180	4.00 × 10^{-4}	750 (500)	3.91	380
$^{40}Ar/^{39}Ar$ hornblende (Harrison 1981)	268	6.00 × 10^{-2}	500	1320	553

*a_s is the effective spherical radius for the diffusion domain. Shown here are typical values. Muscovite and biotite have cylindrical diffusion domains, with typical cylindrical radii shown in parentheses. For these cases, a_s is approximated by multiplying the cylindrical radius by 1.5.
**Ω is equal to $55 D_0 a_s^{-2}$ for Ar thermochronometers.
***$T_{c,10}$ is the effective closure temperature for 10°C Myr^{-1} cooling rate and specified a_s value.

by considering the percentage retention of initial ^4He or ^{40}Ar after being subjected to a stepwise heating event. The loss-only PRZ is defined here by the temperatures associated with 90% and 10% retention for a specified holding time with steady temperatures. The percentage retention corresponds approximately to a similar reduction in the initial age. Note, however, that the loss-only PRZ ignores the production of new ^4He, ^{40}Ar, or FTs. As such, the definition focuses on the ability of a thermochronometer to retain information about old cooling events.

Wolf et al. (1998) defined a different kind of PRZ that accounts for both loss and production. The limits of the loss-and-production PRZ are defined by the temperatures needed to maintain a He, FT, or Ar age equal to 90% or 10% of the hold time for a steady thermal event. The time-temperature conditions associated with 90% and 10% retention are determined using the loss-and-production equation in Wolf et al. (1998), with the initial age set to zero (i.e., setting $^4He^*/P = 0$ in their equation 5). This type of PRZ is useful for understanding the evolution of cooling ages in a borehole. The CLOSURE program calculates both types of PRZs.

The loss-only PRZs for He and Ar dating (**Figure 1*a*,*c***) were calculated using the exact versions of the loss-only diffusion equations given in Fechtig & Kalbitzer (1966) and McDougall & Harrison (1999). The following equations provide approximate solutions,

$$T_{PRZ\,90\%} = \left[\frac{-R}{E_a + PV_a}\ln\left(\frac{\pi a_s^2}{3600 D_0 t}\right)\right]^{-1} \quad \text{and} \tag{2a}$$

$$T_{PRZ\,10\%} = \left[\frac{-R}{E_a + PV_a}\ln\left(\frac{-a_s^2}{\pi^2 D_0 t}\ln\left(\frac{\pi^2}{60}\right)\right)\right]^{-1}, \tag{2b}$$

which match the exact solutions to ~5°C to 10°C. These equations are included here to help illustrate the relationship between the holding time, given as t (s), and the partial retention temperatures, $T_{PRZ\,90\%}$ and $T_{PRZ\,10\%}$. The parameter a_s (m) is the equivalent spherical radius for the diffusion domain size.

For He dating of apatite, titanite, and probably zircon, the size of the diffusion domain scales with the natural size of the dated grain (Reiners & Farley 1999, Farley 2000, Reiners et al. 2004). At least in the case of apatite, diffusion is nearly isotropic,

so it can be modeled using a spherical diffusion geometry. However, apatite and zircon commonly have prismatic shapes, so the grain dimensions need to be converted to an equivalent spherical radius for this calculation. Fechtig & Kalbitzer (1966) and Meesters & Dunai (2002) showed that

$$a_s \approx 3\frac{V}{A}, \tag{3a}$$

where V and A refer to the volume and surface area, respectively, of the dated mineral grain. In contrast, Ar diffusion from most K-feldspars exhibits kinetic properties consistent with a heterogeneous assortment of domains, all of which are smaller than the physical grain size. McDougall & Harrison (1999) estimate that the Ar diffusion domains in K-feldspar have effective radii ranging from 1 to 100 μm.

The domain sizes for Ar diffusion in biotite, muscovite, and hornblende appear to be equivalent to the physical size of the dated grain. [Note that this issue is not fully resolved for biotite, as summarized by McDougall & Harrison (1999).] Argon diffusion is isotropic for hornblende and K-feldspar, so diffusion is modeled using a spherical geometry and a_s is estimated using Equation 3. Biotite and muscovite are anisotropic, with the fast direction of diffusion parallel to the basal plane. Ideally, one should use equations based on a cylindrical diffusion geometry, but we have opted to approximate the solution by converting the cylindrical radius a_c of the mica grains into an equivalent spherical radius, where

$$a_s = 1.5\, a_c, \tag{3b}$$

and then using this radius with the spherical solution for the diffusion equations. This approximation works well for estimating $T_{PRZ\,90\%}$ and effective closure temperatures (introduced below), but less so for $T_{PRZ\,10\%}$.

Apatite, titanite, and zircon are the main minerals dated by the He method. Among all thermochronometers that are currently thought to be well calibrated and understood, the He apatite system has the lowest PRZ temperatures. In fact, our PRZ calculations predict that apatite will lose measurable amounts of He when held at average surface temperatures (~10°C) for longer than ~250 Myr (**Figure 1*a***). Ar dating is usually applied to K-feldspar, biotite, muscovite, and hornblende. Argon in hornblende has the highest PRZ temperatures relative to the other thermochronometers (**Figure 1*c***).

The width of the PRZ increases systematically for those thermochronometers with greater PRZ temperatures. For instance, the He PRZ spans a temperature range of 35°C, whereas the Ar hornblende PRZ has a temperature range of 100°C. This observation is important because cooling ages can become quite complicated if a sample remained for a long time in the PRZ (e.g., Reiners & Farley 2001, House et al. 2002). This possibility is more likely for Ar muscovite and Ar hornblende because of their larger PRZ.

The PRZs for both He and Ar dating are affected by the diffusion domain size, a_s. The examples shown in **Figure 1** are based on typical values for a_s, but grain size may be quite different from typical. The grain size effect can be significant. For example, an increase in a_s for K-feldspar from 10 μm to 100 μm causes an increase in PRZ temperatures of ~40°C. Pressure can also cause an increase in the PRZ temperatures,

Effective closure temperature, T_c: temperature of a rock at its thermochronologic cooling age, assuming a steady monotonic cooling history. For Ar and He thermochronometers, T_c is a function of the activation energy, frequency factor, cooling rate, and geometry and size of the crystal/grain. For FT thermochronometers, T_c is a function of the activation energy, a proportionality constant, and the cooling rate

especially for the higher temperature thermochronometers. For example, McDougall & Harrison (1999) estimate that V_a for biotite and muscovite is about 10 to 14 cm^3 mol^{-1}. An increase in pressure from 0 to 1 GPa (equal to a crustal depth of ~35 km) would cause an increase in the PRZ temperatures for these micas of ~40°C to 50°C. Composition can also influence the PRZ temperatures. For example, Ar retention in biotite appears to increase with increasing concentrations of Fe and F. For hornblende, Ar retention seems to increase with increasing Mg, Al, and Fe^{+3}/Fe^{+2}. In contrast, the PRZ temperatures for He dating of apatite appear to be largely independent of composition.

The retention of FTs is also controlled by diffusion, but the process is more complicated than that for ^{4}He and ^{40}Ar. FT retention is independent of grain size. Diffusion of fission-track defects probably occurs on multiple length scales, all of which are smaller than the length scale of an individual FT. As noted above, FT defects likely have a range of thermal stabilities, which means that FT annealing cannot be represented by a single diffusive process. Experimental studies have shown that the macroscopic activation energy increases with increasing annealing. Thus, the definition of the loss-only PRZ is best determined directly from stepwise-heating experiments. These data are used to define the isopleths for 90% and 10% retention as a function of time and temperature plot and then extrapolated to geologic timescales. The retention isopleths are usually well approximated by the Arrhenius equation,

$$t = \Omega^{-1} \exp\left[-\frac{E_a}{RT}\right] \quad \text{or} \tag{4a}$$

$$\ln[t] = -\ln[\Omega] - \frac{E_a}{RT}, \tag{4b}$$

where Ω (s^{-1}) is a proportionality constant and t (s) is the hold time. Equation 4b is used for FT retention data from stepwise heating experiments. The best-fit result is used to independently estimate Arrhenius parameters for the 90% and 10% retention isopleths (**Table 2**). The loss-only PRZ temperatures are given by

$$T_{PRZ\,90\%} = \frac{-E_{a,90\%}}{R \ln[t\Omega_{90\%}]} \quad \text{and} \tag{5a}$$

$$T_{PRZ\,10\%} = \frac{-E_{a,10\%}}{R \ln[t\Omega_{10\%}]}. \tag{5b}$$

One can see from **Figure 1*b*** that the PRZ temperatures for apatite FT and zircon FT are influenced by several factors. Green et al. (1985) were first to recognize that the FT retention in apatite increased with increasing Cl content. More recent studies suggest that OH, Fe, Mn, and the rare earth elements probably also contribute to increased FT retentivity in apatite (Carlson et al. 1999, Donelick et al. 1999, Ketcham et al. 1999, Barbarand et al. 2003). Recent experimental work by Wendt et al. (2002) suggests that FT retentivity in apatite might increase with increasing pressure. This result is surprising given the good agreement between laboratory and borehole studies for FT retention in apatite (Kohn et al. 2003). Furthermore, there is no pressure effect

Table 2 Closure parameters for He and FT dating

Method (references)	E_a (kJ mol^{-1})	D_0 (cm^2 s^{-1})	a_s^* (μm)	Ω** (s^{-1})	$T_{c,10}$*** (C)
(U-Th)/He apatite (Farley 2000)	138	50	60	7.64×10^7	67
(U-Th)/He zircon (Reiners et al. 2004)	169	0.46	60	7.03×10^5	183
(U-Th)/He titanite (Reiners & Farley 1999)	187	60	150	1.47×10^7	200
FT apatite[1] (average composition[2]) (Ketcham et al. 1999)	147	—	—	2.05×10^6	116
FT Renfrew apatite[3] (low retentivity) (Ketcham et al. 1999)	138	—	—	5.08×10^5	104
FT Tioga apatite[3] (high retentivity) (Ketcham et al. 1999)	187	—	—	1.57×10^8	177
FT zircon[1] (natural, radiation damaged) (Brandon et al. 1998)	208	—	—	1.00×10^8	232
FT zircon (no radiation damaged) (Rahn et al. 2004, fanning model)	321	—	—	5.66×10^{13}	342
FT zircon (Tagami et al. 1998, fanning model)	324	—	—	1.64×10^{14}	338

*a_s is the effective spherical radius for the diffusion domain. Shown here are typical values.

**Ω for FT thermochronometers is measured directly from experimental heating experiments and is equal to $55 D_0 a_s^{-2}$ for He and Ar thermochronometers.

***$T_{c,10}$ is the effective closure temperature for 10°C Myr^{-1} cooling rate and the specified a_s value.

[1]Recommended values for most geologic applications.

[2]Average composition was taken from table 4 in Carlson et al. (1999). Equation 6 in Carlson et al. (1999) was used to estimate $r_{mr0} = 0.810$ for this composition. Closure parameters were then estimated using the HeFTy program (Ketcham 2005).

[3]Closure parameters were estimated from HeFTy and $r_{mr0} = 0.8464$ and 0.1398 for Renfrew and Tioga apatites, respectively, as reported in Ketcham et al. (1999).

observed for FT retention in zircon (discussed below). More experiments are needed before this new result can be adequately assessed.

There has been much interest in finding an easily measured retention index or kinetic factor so that one could scale the retention behavior of FTs. Almost all of this work has focused on FTs in apatite. The D_{par} and r_{mr0} parameters of Ketcham et al. (1999) and Donelick et al. (1999) represent important steps toward this objective, but neither is able to provide confident predictions of FT retentivity over the full range of apatite compositions. Further progress on this problem would be aided by a better understanding of the atomic-scale processes associated with FT annealing. Carlson (1990) proposed the first mechanistic model for FT annealing, but Ketcham et al. (1999) have demonstrated significant deficiencies with the Carlson model.

We use the average apatite from Carlson et al. (1999) to define a reference for the FT retention of a typical apatite, as one might find in a sample of detrital apatites from sandstone. Their equation 6 was used to estimate the retention parameter r_{mr0} for this average apatite composition and that parameter was then used with the HeFTy program (Ketcham 2005) to estimate the parameters in **Table 3** for the loss-only PRZ. We used this same approach for the Renfrew and Tioga apatites, which Carlson et al. (1999) considered to be the least and most retentive, respectively, of the common naturally occurring apatites in their study. The average apatite has F:Cl:OH = 77:3:20 (numbers indicate the percent of cation substitution in the F site), and is thus mainly a fluorapatite, with some OH substitution. The Renfrew apatite is a

Table 3 Parameters for FT partial retention zones

Method (references)	Retention level	E_a (kJ mol^{-1})	Ω^1 (s^{-1})
FT apatite[2] (average composition[3])	90%	127	2.67×10^5
(Ketcham et al. 1999)	10%	161	1.55×10^7
FT Renfrew apatite[4] (low retentivity)	90%	124	1.91×10^5
(Ketcham et al. 1999)	10%	150	4.39×10^6
FT Tioga apatite[4] (high retentivity)	90%	140	1.41×10^6
(Ketcham et al. 1999)	10%	232	3.38×10^{10}
FT Durango apatite	90%	160	1.02×10^{12}
(Laslett et al. 1987, Green 1988)	10%	195	2.07×10^{12}
FT zircon[2] (natural, radiation damaged)	90%	225	2.62×10^{11}
(Brandon et al. 1998)	10%	221	1.24×10^8
FT zircon (no radiation damage)	90%	272	5.66×10^{13}
(Rahn et al. 2004, fanning model)	10%	339	5.66×10^{13}
FT zircon	90%	231	1.09×10^{12}
(Tagami et al. 1998, fanning model)	10%	359	1.02×10^{15}

[1] Ω for FT thermochronometers is measured directly from experimental heating experiments.
[2] Recommended values for most geologic applications.
[3] Average composition was taken from **Table 4** in Carlson et al. (1999). Equation 6 in Carlson et al. (1999) was used to estimate $r_{mr0} = 0.810$ for this composition. PRZ parameters were then estimated using the HeFTy program (Ketcham 2005).
[4] PRZ parameters were estimated from HeFTy and $r_{mr0} = 0.8464$ and 0.1398 for Renfrew and Tioga apatites, respectively, as reported in Ketcham et al. (1999).

nearly end-member fluorapatite, with F:Cl:OH = 97.5:0.5:2. The Tioga apatite is a mixed fluor/hydroxylapatite, with F:Cl:OH = 44:8:46 and 0.6% substitution of Fe^{+2} into the Ca cation site. **Figure 1*b*** shows that the average apatite and the Renfrew apatite have similar PRZs. The Tioga apatite is much more retentive than the average apatite, with $T_{PRZ10\%}$ about 100°C greater.

This comparison indicates why variable FT retentivity in apatite is generally not a major problem. Fluorapatites have the lowest FT retentivity among all apatites, and most naturally occurring apatites have compositions close to that of an end-member fluorapatite. In contrast, increased retentivity can occur by several types of substitution, with Cl and OH substitution being the most important. Care is needed to screen for highly retentive apatites, a task that is especially important when dating detrital apatites from sedimentary rocks.

Zircon also shows a range in FT retention (**Figure 1*b***). The main factor appears to be radiation damage by alpha decay (Nasdala et al. 2001, Ewing et al. 2003), which causes a decrease in FT retentivity (Kasuya & Naeser 1988). Compositional effects have not been recognized. Several experimental studies have shown that pressure has no significant influence on retentivity (Fleischer et al. 1965, Brix et al. 2002, Yamada et al. 2003). Rahn et al. (2004) estimated a no-damage PRZ using a compilation of published annealing experiments done on damage-free zircons. The natural radiation

damage in these zircons was removed by heating, and then neutron irradiation was used to induce new FTs. Brandon et al. (1998) estimated a PRZ for natural radiation-damaged zircon using 1-h annealing experiments from Tagami et al. (1990), and a downhole suite of ZFT ages from a deep borehole in Germany (Zaun & Wagner 1985). They also compared the estimated PRZ with other field-based constraints, including estimates of closure temperature from other thermochronometers (discussed below). The zero-damage zircons indicate a $T_{PRZ10\%}$ that is ~125°C greater than that estimated for natural radiation-damaged zircon. The PRZ labeled by Tagami et al. was estimated from a comprehensive laboratory study of FT annealing in natural zircon from a 21-Ma dacite tuff (Yamada et al. 1995, Tagami et al. 1998). Notably, the 10% retention isopleth for this study of radiation-damaged zircon is identical to that for the zero-damage zircon reported by Rahn et al. (2004) (**Figure 1*b***). In laboratory heating experiments, alpha radiation damage appears to anneal at lower temperatures than FTs (Tagami et al. 1998). Garver & Kamp (2002) have shown that, at geologic timescales, alpha radiation damage, at least as indicated by zircon color, is retained at temperatures above the FT PRZ. When calibrating thermochronometers, there is no automatic assurance that diffusion and annealing studies conducted at laboratory timescales will be applicable at geologic timescales. We conclude for zircon FTs that retentivity changes with time owing to changes in the thermal stability of alpha damage. At geologic timescales, alpha damage is able to persist to high temperatures where it reduces the retentivity of associated FTs. Rahn et al. (2004) argued that the naturally calibrated PRZ is probably appropriate for most geologic settings. However, the zero-damage PRZ would be more appropriate for settings where the rocks have rapidly cooled from high initial temperatures (>350 to 400°C). In this case, there would be no time to form alpha damage. High-temperature metamorphic core complexes might be a typical example.

EFFECTIVE CLOSURE TEMPERATURE

Dodson (1973, 1979) published an analytical solution for the evolution of a thermochronometer that cools at a steady rate and whose retention behavior is controlled by thermally activated diffusion. His solution provides an estimate of the effective closure temperature, T_c, defined as the temperature of the dated mineral at the time indicated by the thermochronometer. We know that a thermochronometer closes over a temperature range (as suggested by our PRZ estimates), but the measured cooling age will, by definition, point to just a single temperature on the cooling path.

We emphasize that T_c is only defined for the case of steady cooling through the PRZ, but this assumption is reasonable for eroding mountain belts, given the narrow temperature range for the PRZ and the slow response of the thermal field to external changes. In contrast, this assumption will likely fail and T_c will have little meaning in cases involving reheating by local igneous intrusions, hydrothermal circulation, or depositional burial.

Dodson (1973, 1979) estimated T_c using

$$\dot{T} = \frac{\Omega R T_c^2}{E_a + PV_a} \exp\left[\frac{-E_a - PV_a}{RT_c}\right], \quad (7)$$

where $\dot{T}$ is the cooling rate, and Ω and E_a are closure parameters, as defined in **Tables 1** and **2**. The PV_a is included for completeness, but the influence of pressure is generally taken to be negligible, as noted before.

For He and Ar dating, $\Omega = \frac{55 D_0}{a_s}$, where a_s is the equivalent spherical radius for the diffusion domain. E_a and D_0 are given in **Tables 1** and **2**, along with typical values for a_s. The relationships discussed with Equations 3a and 3b above can be used to make specific estimates for a_s.

Dodson (1979) outlines the use of Equation 7 for estimating T_c for FT dating. He recognized that FT annealing does not follow a first-order rate law (Green et al. 1988). He argued that the 50% retention isopleth should provide reasonable estimates for E_a and Ω in Equation 7. This approach makes sense given that the steady monotonic cooling path used for the closure temperature solution must pass through the full PRZ and thus would sample the full range of variation in the retention isopleths. The estimation of these parameters is the same as shown for Equation 5, but in this case, the fitting is done using the 50% retention isopleth. T_c can be estimated directly using a track-modeling program, such as HeFTy (Ketcham et al. 1999, Ketcham 2005). We have found that the T_c estimated by track-modeling programs is nearly identical (± 1°C) to that given by the Dodson equation.

Kohn et al. (2003) claimed that the effective closure temperature concept does not apply to FT dating. FT dating is commonly used to determine thermal histories for sedimentary basins, where the time-temperature path can include both heating and cooling within the PRZ. We agree that the closure temperature concept does not apply in this case, but this point holds for any thermochronometer where cooling through the PRZ is not steady and monotonic. Other methods, such as the HeFTy program, are needed to interpret the thermal histories. Nonetheless, we find that T_c is useful for thermochronologic studies of erosion and exhumation in mountain belts where steady monotonic cooling through the PRZ tends to be the rule, rather than the exception.

Figure 2*a* shows T_c as a function of cooling rate for the He, FT, and Ar thermochronometers, using the parameters from **Tables 1** and **2**. The cooling rate has an important effect on the relationship between cooling age and erosion rate, as discussed below. The general rule is that T_c increases with increasing cooling rate. Furthermore, the cooling rate effect becomes more pronounced with increasing retentivity of the thermochronometer. For instance, T_c for the apatite He system increases ~13°C per tenfold increase in cooling rate, whereas T_c for the hornblende Ar system increases ~43°C for the same cooling rate increase.

We note that for some minerals, in certain circumstances crystallization temperatures could potentially be similar to or even lower than the nominal T_c. For example, white mica and K-feldspar can crystallize at temperatures well below their respective T_c values. In this case, the age of the thermochronometer would record the time of crystallization. Although some thermal history constraints may still be possible in

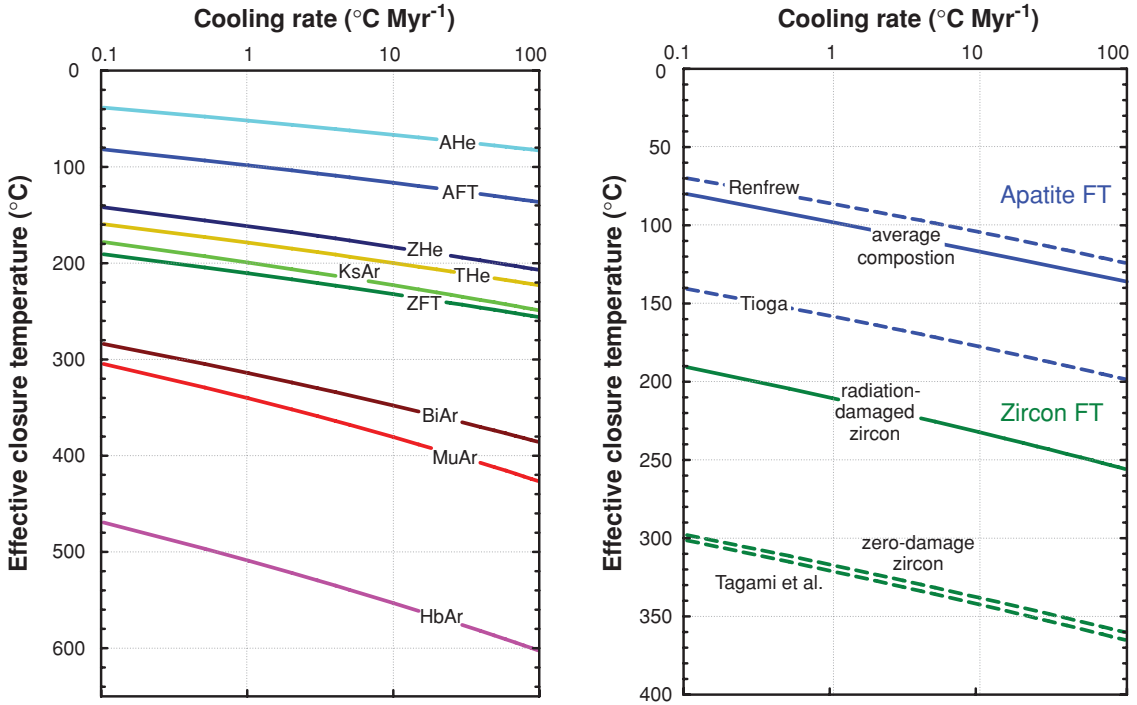

Figure 2

Effective closure temperature (T_c) as a function of cooling rate for common He, FT, and Ar thermochronometers. Estimates shown here are based on Equation 7 and parameters in **Tables 1–2**. Results were calculated using the CLOSURE program.

such cases, the closure temperature concept does not strictly apply, and this could potentially confound attempts to relate thermal and exhumational histories. This underscores the need to consider the conditions of a mineral's formation, as well as its cooling path, in interpreting thermochronologic histories.

Figure 2*b* provides a comparison of the various T_c estimates for apatite and zircon FT dating. T_c for the average apatite is only ~10°C higher than that for an end-member fluorapatite, as represented by the Renfrew apatite. In contrast, the T_c for the Tioga apatite is ~60°C above that for the average apatite. This range in T_c would give a 7 Myr spread of FT ages for a typical orogenic cooling rate of ~10°C Myr^{-1}. FT dating of detrital apatites in thermally reset sandstones commonly yields over-dispersed grain ages, which means that the range of grain ages is much greater than expected owing to analytical errors alone. This result is probably a consequence of a mix of apatite compositions, which gives a mix of retention behaviors. The T_c estimates shown here indicate that the youngest grains in a grain age distribution should be dominated by low-retentivity apatites. Peak-fitting methods can be used to isolate the minimum age, which is the age of the youngest fraction of grain ages (Galbraith & Green 1990; Galbraith & Laslett 1993; Brandon 2005, as summarized

in Ehlers et al. 2005). This approach provides a reliable way to isolate the FT age of the less retentive apatites in a reset grain-age distribution (Brandon et al. 1998, Zattin et al. 2002).

Figure 2*b* also illustrates the range of T_c estimates for the zircon FT system. We have already noted that the FT retention in zircon appears to be strongly influenced by radiation damage. The T_c estimates for zircon FT annealing experiments of Tagami et al. (1998) are nearly identical to those for the zero-damage zircons of Rahn et al. (2004). Annealing in natural radiation-damaged zircons indicates T_c values that are lower by ~110°C (Brandon et al. 1998). There are at least three studies that have used cross-calibration between different thermochronometers to make field-based estimates of T_c for the zircon FT system (Harrison et al. 1979, Hurford 1986, Foster et al. 1996). All agree closely with predictions based on natural radiation-damaged zircon (see compilation in Brandon et al. 1998). The T_c for zero-damage zircons may be applicable to settings where the zircons cooled rapidly from high initial temperatures (>350 to 400°C), given that there would be little alpha damage in these zircons during closure.

EROSION, TEMPERATURE, AND COOLING AGE

Our objective here is to illustrate the relationship between erosion rates and cooling ages. As a first step, it is necessary to consider how the thermal profile in the crust is affected by erosion. Consider a one-dimensional steady-state thermal field in an infinite layer of thickness L. The base and top of the layer are held at constant temperatures of T_L and T_S, respectively. Material moves through the layer at a constant velocity w. This situation simulates a steady-state orogen where accretion at the base of the orogen is balanced by surface erosion at the same rate, so that $w = \dot{\varepsilon}$, where $\dot{\varepsilon}$ is erosion rate. The thickness of the orogen remains steady and the vertical velocity through the orogen is approximately uniform and steady.

This upper surface of the model is equivalent to the mean elevation of the local topography in the study area. It is well known that isothermal surfaces will tend to follow the long-wavelength form of the topography (Braun, 2002). Those perturbations are centered, however, on the depth predicted by the one-dimensional solution here. Thus, one can think of this solution as providing a description of the mean depth of the isothermal surfaces, relative to the mean elevation of the overlying topography. (The influence of topography on thermal structure is discussed in more detail below.)

Batt & Brandon (2002) show that this one-dimensional, steady-state solution provides a good approximation even when the horizontal velocities in the orogen are significant. Incoming accreted material is assumed to maintain the base of the orogen at a fixed temperature, as represented by T_L at a depth L. Most thermochronometers have closure isotherms that are shallower than ~10 to 15 km. We have found that the thermal structure in the upper part of the one-dimensional solution is fairly insensitive to the thickness of the layer and to the nature of the basal boundary condition, as long as L is at least two or three times the closure depth. Thus, the solution works well for the He and FT thermochronometers and less well for the Ar thermochronometers.

The Peclet number, $P_e = \frac{\dot{\varepsilon} L}{\kappa}$, is used to choose between two one-dimensional thermal solutions, where κ is the average thermal diffusivity of the layer. The first solution accounts for heat transport associated with erosion, which becomes significant when P_e is significantly greater than zero,

$$T(z) = T_S + \left(T_L - T_S + \frac{H_T L}{\dot{\varepsilon}}\right) \frac{1 - \exp(-\dot{\varepsilon} z/\kappa)}{1 - \exp(-\dot{\varepsilon} L/\kappa)} - \frac{H_T z}{\dot{\varepsilon}}, \quad (8a)$$

where z is depth. As P_e approaches zero, the solution is given by

$$T(z) = T_S + \frac{(T_L - T_S)z}{L} + \frac{H_T z(L - z)}{2\kappa}. \quad (8b)$$

The layer is assigned a uniform internal heat production H_T, which is specified in units of $^\circ$C Myr^{-1}. The more common practice is to use an exponentially decreasing heat production, but this approach seems inappropriate for many convergent orogens where the crust is composed mainly of recently accreted rocks. **Figure 3** shows the thermal profile as a function of different steady erosion rates.

Erosion causes temperatures to increase in the upper part of the crust. We use thermal parameters for the northern Apennines of Italy for the examples calculated here. The Apennines represents a fairly typical convergent orogen (Vai & Martini 2001). We estimate that $L = 30$ km, $\kappa = 27.4$ km^2 Myr^{-1}, and $T_S = 14^\circ$C. In areas without erosion, the surface thermal gradient is $\sim 20^\circ$C km^{-1}, which is equal to a "no-erosion" surface heat flux $Q_S = 40$ mW m^{-2}. Our estimates of the internal heat production and the temperature at the base of the layer were guided by pressure-temperature estimates of deeply exhumed metamorphic rocks exposed within the orogen and the observed "no-erosion" surface heat flux. Our estimate for uniform internal heat production H_T is 4.5°C Myr^{-1}, which is equal to a volumetric heat production of 0.33 μW m^{-3}. T_L is estimated to be $\sim 540^\circ$C.

Next, we consider the effect of erosion rate on the depth of the effective closure temperature. Equation 8 provides a full description of the temperature and thermal gradient as a function of depth. The cooling rate is given by $\dot{T}(z) = \dot{\varepsilon} \frac{\partial T}{\partial z}$. The Dodson equation (Equation 7) provides a second equation relating T_c to $\dot{T}$. An iterative search is used to find the depth z_c, which satisfies both equations; z_c corresponds to T_c and thus marks the depth of effective closure. The predicted cooling age is given by $\frac{z_c}{\dot{\varepsilon}}$. Note that this z_c is referenced to the mean elevation h_m of the local topography. Samples reaching the surface at elevations h other than the mean elevation will have predicted ages equal to $\frac{h - h_m + z_c}{\dot{\varepsilon}}$ (Brandon et al. 1998, Reiners et al. 2003b).

The colored lines in **Figure 3** show z_c and T_c for the He apatite, FT zircon, and Ar muscovite thermochronometers as a function of erosion rate. There are two competing effects that determine the depth of the closure isotherm. Faster erosion causes all isotherms to migrate closer to the surface, but the steeper thermal gradient causes faster cooling and a larger T_c. Thus, the closure depth becomes shallower with faster erosion, but this response is offset by the increase in T_c caused by faster cooling.

The relationship between erosion rate and cooling age for samples at the mean local elevation ($h = h_m$) is shown in **Figure 4**. For slow erosion ($<\sim 1$ km Myr^{-1}),

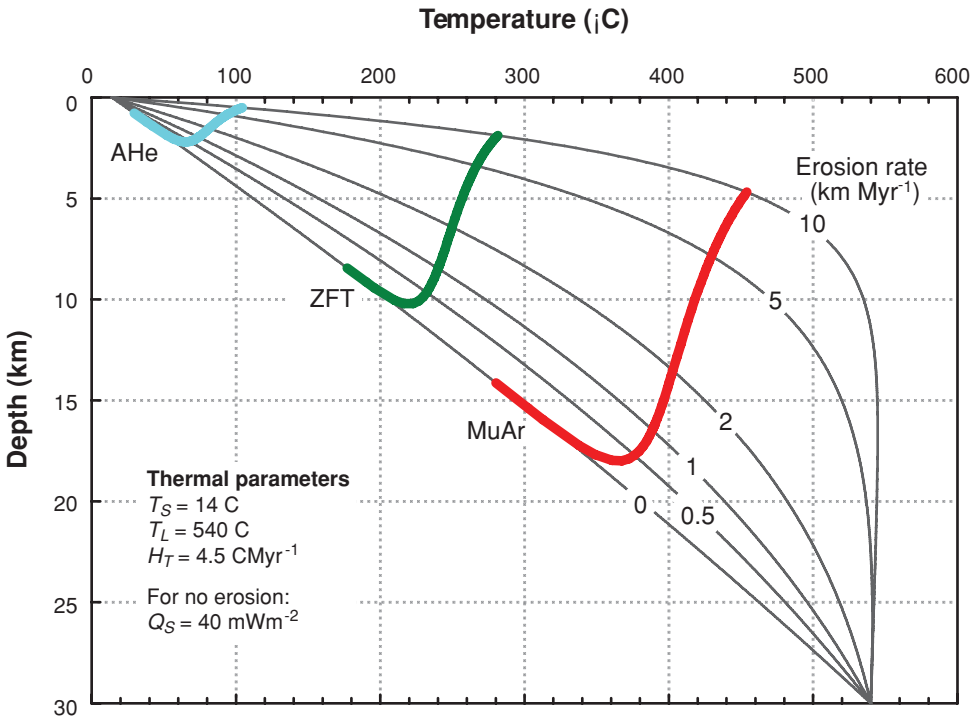

Figure 3

Influence of erosion rate on the thermal profile and closure temperatures at steady state. The thermal profiles are steady-state solutions for a one-dimensional thermal field with a steady erosion rate. Temperature is held fixed at the top and bottom of a 30-km thick infinite layer. Erosion is represented by a steady velocity through the layer. The specific thermal parameters used for this model are based on the northern Apennines of Italy, which is a fairly typical convergent orogen. The color lines show the effective closure temperature for apatite He (AHe), zircon fission track (ZFT), and muscovite Ar (MuAr) as a function of increasing erosion rate. The results were determined from the AGE2EDOT program, using the following procedure: For a specified erosion rate, the program finds the associated steady-state thermal profile and the cooling rates for that profile. The Dodson Equation (Equation 7) is then used with the parameters from **Tables 1** and **2** to find the temperature and depth of effective closure for the thermochronometer of interest. This is repeated for many closely spaced profiles to give the continuous closure temperature curves shown in the figure.

erosion rate and cooling age change proportionally. For example, if we double the erosion rate from 0.1 to 0.2 km Myr^{-1}, He apatite cooling ages would decrease by half, from 20 to 10 Ma. This proportionality is expected when erosion rates are too slow to move the closure isotherm. Now consider doubling of the erosion rate from 1 to 2 km Myr^{-1}. The He apatite age decreases by more than half, from 2 to 0.7 Ma. In this case, the erosion rates are fast enough to significantly change the depth of the closure isotherm. In fact, note that the slopes of the curves are 1:1 in the log-log plot

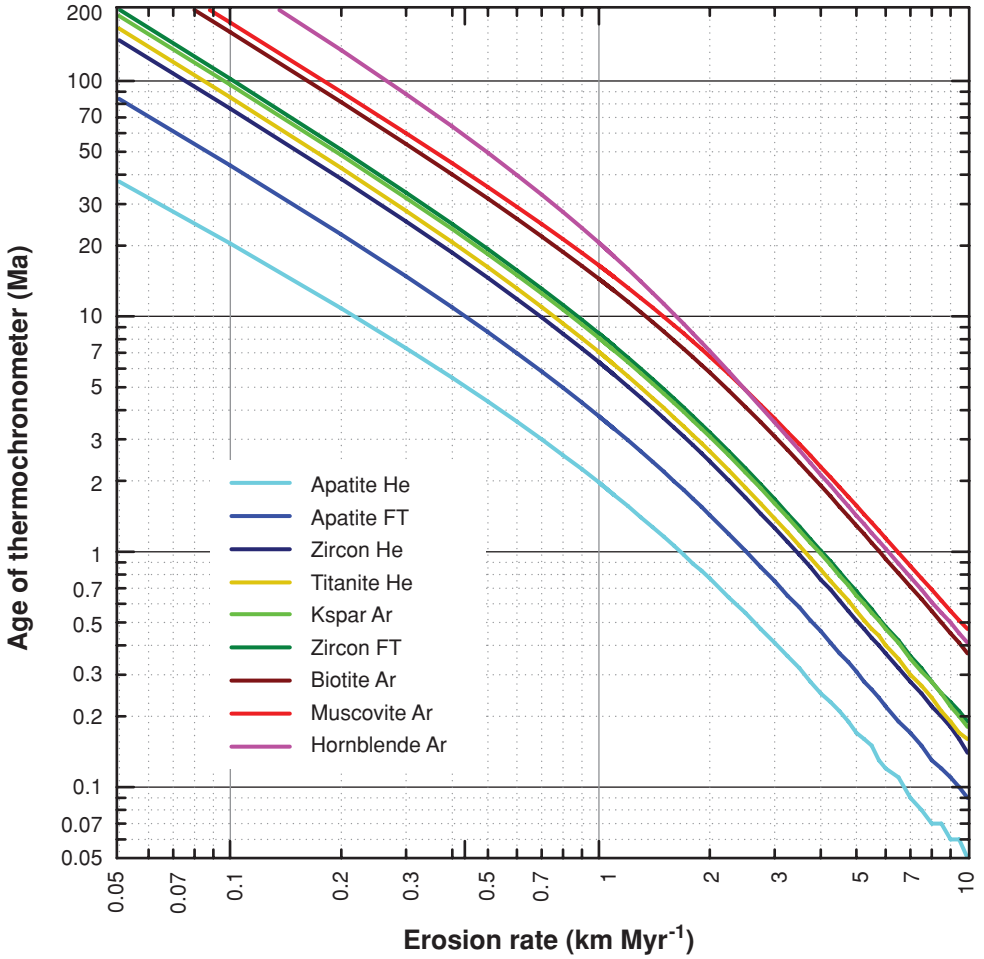

Figure 4

Relationship of cooling ages to erosion rates at exhumational steady state for common He, FT, and Ar thermochronometers. Results were determined using the AGE2EDOT program. The thermal field is represented by a one-dimensional steady-state thermal field, as shown in **Figure 3**. Closure parameters are from **Tables 1** and **2**. The thermal parameters are based on the northern Apennines.

where erosion rates are slow. This situation indicates that that heat transport is mainly occurring by conduction. The steeper slopes at higher erosion rates indicate that a significant fraction of the heat moving through the layer is being carried advectively by the velocity of the rock toward the surface. Moore & England (2001) provide a detailed analysis of the thermal part of this problem, but they did not include the effect of cooling rate on closure temperature.

TIME TO EXHUMATIONAL STEADY STATE

The steady-state condition used above may seem overly simplistic. In fact, we know that the thermal profile requires time to reach steady state, especially for the deeper parts of the profile. For thermochronologic interpretation, we are not interested in a full thermal steady state, but rather in an exhumational steady state (Willett & Brandon 2002). Exhumational steady state means that the products of exhumation have become steady with time. For example, Bernet et al. (2001) argued that the central part of the Swiss Alps has been shedding zircons with a steady FT age since ~25 Ma. This implies that both the exhumation rate and the closure depth have remained steady with time. We can define exhumational steady state using the normalized velocity of the closure isotherm, which is defined by the vertical velocity of the isotherm divided by the erosion rate. A normalized velocity of zero means that the closure isotherm has reached a steady-state position, whereas a normalized velocity of one means that the isotherm is moving upward at the same rate as the rock. There would be no cooling for this case.

Figure 5 shows the evolution of closure isotherms for He, FT, and Ar thermochronometers as a function of a stepwise increase in erosion rates from zero to a steady rate of 1 km Myr^{-1}. The normalized velocity of the closure isotherm is shown on the vertical axis. The normalized velocity for He apatite and FT apatite systems drops to 10% within 2.5 and 4 Myr, respectively, whereas it takes 8 Myr for the Ar muscovite system to reach this state. Thus, we can expect that the lowest temperature thermochronometers will reach exhumational steady state within a short period of time. It is important to note that, in nature, erosion rates probably do not change in a stepwise fashion. Slower changes will allow the closure isotherm to more closely follow the steady state solution shown in **Figure 3**.

TEMPORAL CHANGES IN EROSION: VERTICAL TRANSECTS

Erosion rates can vary with time and, in some cases, this temporal variation is of prime interest. One approach to constraining changes in erosion rates is to measure cooling ages of systems with different closure temperatures in the same rock. Combining the FT and (U-Th)/He systems on zircon and apatite from the same rock, for example, would provide cooling ages through temperatures of roughly 240°C, 180°C, 110°C, and 65°C, assuming a cooling rate on the order of 10°C Myr^{-1}. Cooling rates between the ages of any system pair can simply be calculated by dividing the difference in the closure temperatures by the difference in cooling ages. A simplistic estimate of the average erosion rate, can then be made by dividing the cooling rate by an assumed geothermal gradient. The geothermal gradient represents a major assumption in this calculation. As described above, erosion causes upward migration of isotherms, increasing the geothermal gradient, especially at shallow depths. If erosion is known to have been steady for a sufficiently long time to establish a steady-state thermal field, this isothermal compression can be accounted for, to first order, by assuming variable geothermal gradient as a function of depth. But if a constant exhumation rate

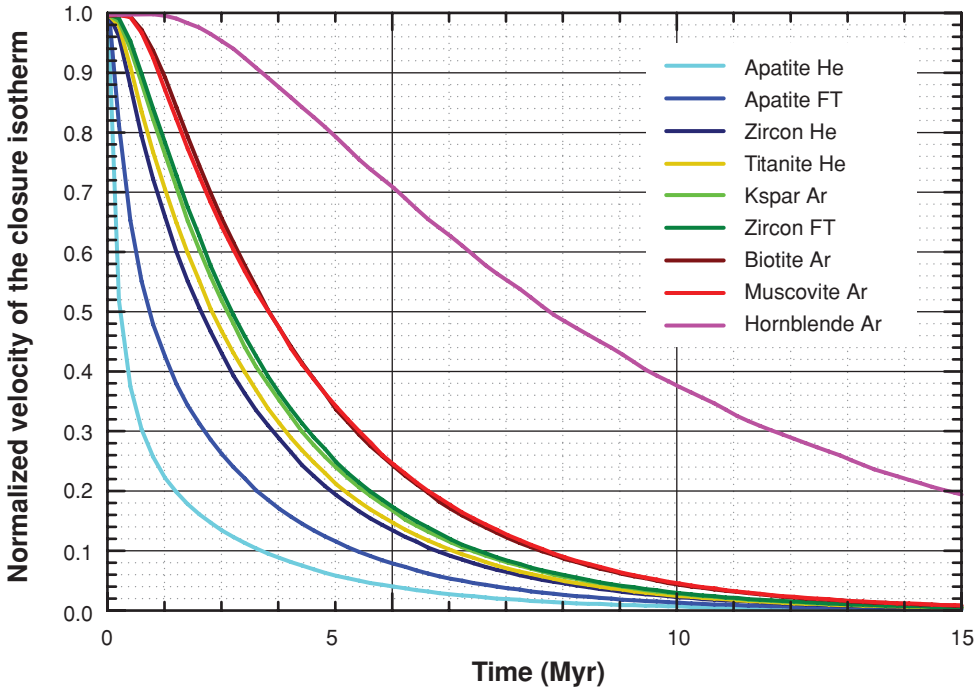

Figure 5

Response of the closure isotherm to the sudden onset of rapid erosion from 0 to 1 km/Myr. Results were determined using the RESPTIME program. The curves show the normalized velocity of closure isotherms with time after the initiation of rapid erosion for the common He, FT, and Ar thermochronometers. The normalized velocity is defined as the vertical velocity of the closure isotherm divided by the erosion rate. A normalized velocity of one means that the closure isotherm is moving with the same velocity as the rock relative to the surface. A normalized velocity of zero means that the closure isotherm has reached its steady-state depth. The thermal calculation is the same as before, except for the introduction of a finite-difference algorithm, which is needed to calculate the time evolution of the thermal profile. The thermal parameters are based on the northern Apennines. Closure parameters are from **Tables 1** and **2**.

has not proceeded long enough to establish a steady-state thermal field, the evolving thermal field will add additional complexity. Moore & England (2001) showed that for some time after a stepwise increase in erosion rate, cooling ages give the appearance of gradually increasing erosion rates with time. This result is an artifact of the migration of the closure isotherm to a new steady state depth (**Figure 5**).

An alternative approach that avoids some of the complications associated with an assumed geothermal gradient would be to examine bedrock cooling ages as a function of depth in an orogen. Obviously, without drilling to depths of at least several hundred meters it is not possible to sample a truly vertical transect. But mountainous regions often provide an approximation of this sampling approach. In some settings, rapid tectonic denudation by normal faulting, combined by isostatically induced tilting, has

exposed deeply exhumed footwall blocks that can be interpreted as inclined crustal sections through depths as great as ∼15 km. In some cases, fossil PRZs are observed at depths that are consistent with reasonable preexhumation geothermal gradients, and cooling ages at greater depths record the onset and rate of tectonic exhumation (Reiners et al. 2000, Stockli et al. 2000, Stockli 2005).

AER: age-elevation relationship

In orogens dominated by erosional denudation, however, topographic relief may be taken to approximate crustal depth, with a vertical transect approximated by bedrock cooling ages measured from samples over a large elevation difference and a relatively short horizontal distance. The vertical transect method will commonly yield a simple age-elevation relationship (AER) that can be interpreted as the vertical velocity of the rocks relative to the closure isotherm at the time of closure. Changes in the slope of the AER with elevation are typically interpreted to represent changes in erosion rate with time. This method was first proposed and used by Wagner & Reimer (1972) and Wagner et al. (1977). Fitzgerald et al. (1995) provide a good review of this method. The vertical transect approach is based on three important assumptions: (*a*) that the closure isotherm was flat at the time of closure; (*b*) at a given time, erosion rates were the same for samples composing the AER (spatially uniform erosion rate); and (*c*) the depth of the closure isotherm has remained constant, so that cooling of rocks can be accurately considered to represent their movement, relative to the surface, through a stationary isotherm.

Figure 6 shows an example of FT and (U-Th)/He cooling ages from rocks of the Coast Plutonic Complex in southeastern Alaska. This transect, collected over a horizontal distance of about 7 km, up the side of Mt. Hefty, has ∼1.8 km of vertical relief (Donelick 1986, Hickes 2001). FT and ZHe ages vary between 40 and 60 Ma and show a steep trend of elevation relative to age, whereas AHe ages show a more gentle trend. The overall slope of the AER for the AHe ages is 0.078 ± 0.004 km Myr^{-1}. If the assumptions above are met, then this estimate indicates the rate of erosion at the time the rocks moved through the AHe closure isotherm (16–38 Ma). Variations in the slope of the AER between any two points in the transect could be interpreted to represent variations in exhumation rates at those times, but in this case such variation is not distinguishable from random error.

The AHe data also provide indirect constraints on the average erosion rate for the time of closure of the cooling ages to present. The closure depth is determined relative to the local mean elevation of the landscape. We define τ_m as the cooling age at the present local mean elevation. The mean amount of eroded section from τ_m to present is equal to the z_c at the time that τ_m closed. For our example, τ_m for AHe is 20 Ma and the erosion rate at that time was 0.08 km Myr^{-1} as indicated by the slope of the AER. The exhumational steady-state solution (**Figure 4**) predicts that at this erosion rate, $T_c = 55°$C and z_c would be 2.0 km, with an average thermal gradient of $(55°\text{C} - 10°\text{C})/2$ km $= 22.5°$C/km (assuming a surface temperature of 10°C km). The predicted average erosion rate is 2.0 km/20 Ma $= 0.1$ km Myr^{-1} for the interval from 20 Ma to present. The AER profile for the AHe ages, which is representative of erosion rates for the interval 38 to 16 Ma, indicates a similar rate of 0.08 km Myr^{-1}. Thus, the assumption of steady erosion is supported by the data.

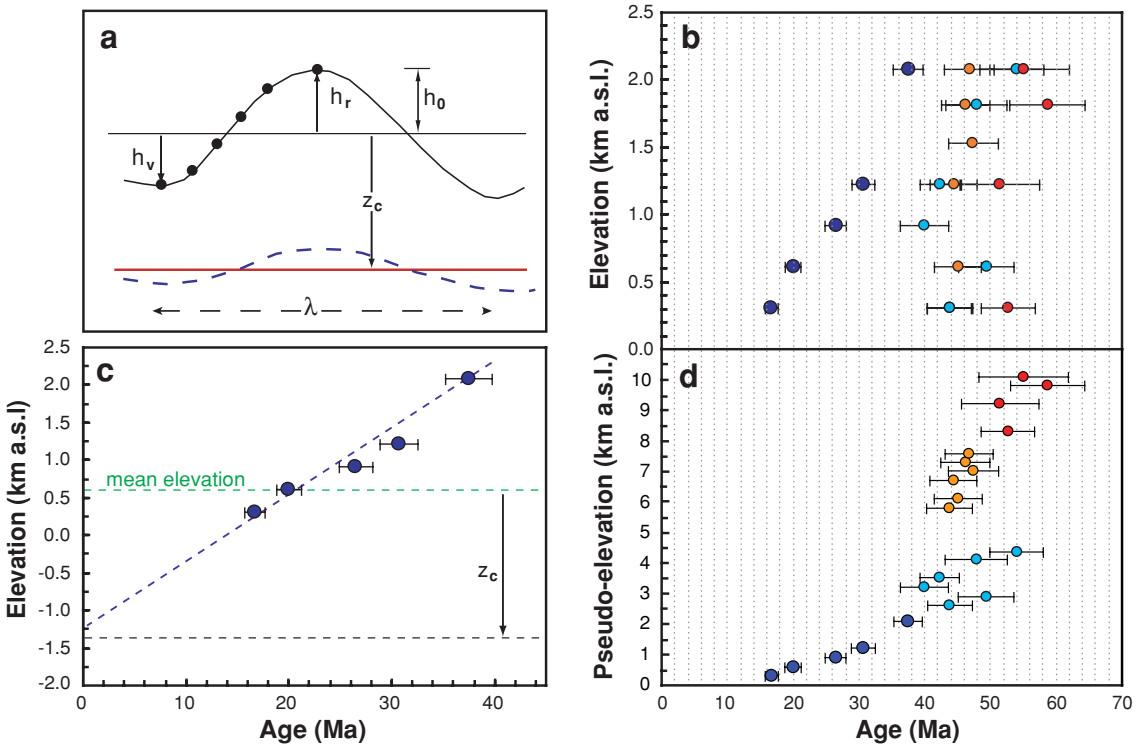

Figure 6

Concepts underlying, and examples of, a thermochronologic vertical transect. (*a*) Samples (*filled circles*) are collected over a range of elevation and a small horizontal distance, i.e., valley bottom to ridge top, over topography with amplitude h_0 and wavelength λ. Consider the case of a steady erosion rate $\dot{\varepsilon}$ through a flat closure isotherm (*solid red line*) at a depth z_c. below the mean elevation h_m. Two samples exposed at different elevations h_r and h_v would have a difference in age of $(h_r - h_v)/\dot{\varepsilon}$. (*b*) ZFT (*red*), ZHe (*orange*), AFT (*light blue*), and AHe (*dark blue*) ages for samples from a vertical transect with 1.8 km of relief, collected over ~7 km horizontal distance, on Mt. Hefty, southeastern Alaska (data from Donelick 1986, Hickes 2001). Regression through the AHe data indicates an exhumation rate of 0.078 $\pm$ 0.004 km Myr^{-1} between ~38 and 16 Ma. (*c*) The average erosion rate after closure is equal to z_c/τ_m, where τ_m is the cooling age at the mean elevation in the landscape, which gives 0.10 km Myr^{-1} for 20 Ma to present (see text for details). (*d*) Stacked pseudovertical transect. AHe ages are plotted in the normal way, but the other cooling ages are offset upward from their true elevations by a height equal to the difference in z_c for that thermochronometer relative to z_c for the AHe system.

Some studies have compared the zero-age intercept of the observed AER trend to the predicted closure depth, based on modern heat flow data, to estimate erosion rates during the interval between cooling ages and present (Parrish 1983, Farley et al. 2001). This approach is essentially the same as the one above, because the estimate of z_c represents the predicted depth where the relevant thermochronometer would

show zero ages. Our approach and that used by Parrish (1983) are both based on a one-dimensional steady-state thermal model (e.g., Equation 8). We both use the modern "no-erosion" surface heat flux with the assumption that this quantity has not changed since τ_m. For the example above, the extrapolated AER trend intersects the elevation axis at our estimate of z_c for AHe (**Figure 6*c***), indicating that there is no significant difference in erosion rates over the intervals 38–16 Ma and 20 Ma to the present. If the zero-age intercept of the AER trend was at an elevation significantly above (below) the estimate closure depth, this would be evidence that erosion rates had increased (decreased) after the ages of the samples composing the AER. The difference between the erosion rate inferred from the AER and the more recent one would be the difference in predicted closure depth and observed extrapolated intercept, divided by the inferred time of erosion rate change. Alternatively, a mismatch in predicted closure depth and zero-age intercept might indicate that our assumption of a steady "no-erosion" surface heat flux is wrong.

We can extend the AER by adding cooling ages for higher-temperature thermochronometers. This approach involves construction of a stacked pseudo-vertical transect (Reiners et al. 2003b), as shown in **Figure 6*d***. The AHe ages are plotted in the normal way, as a function of age and elevation. The cooling ages for the other thermochronometers are plotted with their elevations shifted upward by an amount equal to the difference in z_c for the thermochronometer relative to that for the AHe thermochronometer. We use the AGE2EDOT program to estimate closure depths of 2.2 km for AHe, 4.5 km for AFT, 7.7 km for ZHe, and 10.2 km for ZFT. These depths are predicted using the same thermal parameters as for the examples above (e.g., **Figure 5**) and a steady erosion rate of 0.1 to 0.3 km Myr^{-1}. The z_c estimates are fairly insensitive to the assumed erosion rate given the slow erosion for this area. The stacked pseudovertical transect for the ZFT, ZHe, AFT, and AHe systems (**Figure 6*d***) shows that prior to 40 Ma, erosion was much faster, at a rate of ~0.5 km/Myr.

Interpretations of exhumation rates and their changes through time by these approaches can provide insights to the long-term evolution of orogens with sufficient topographic relief, but they are limited by the assumptions described above. One of the most important of these assumptions is that the closure isotherm is flat and not bent by topography (**Figure 6*a***). Closure isotherms are likely to have significant topography where the closure temperature is low, the exhumation rate is high, or the topography over which samples are collected has a long effective wavelength. As shown by numerous studies, violation of the flat closure isotherm assumption (in the case of no relief change) has the general effect of rotating the AER to a steeper trend, resulting in a high-side bias for the erosion rates measured from the AER (Stuwe et al. 1994, Mancktelow & Grasemann 1997, Braun 2002, Reiners et al. 2003b). For the AHe and AFT systems, topography with wavelengths greater than about 10 km and 18 km, respectively, has the effect of bending closure isotherms by more than about 20%, which will cause a similar (~20%) upward bias in the exhumation rate estimated directly from an AER. The sensitivity of closure isotherms of these systems to topography has also been used to an advantage, however, by studies examining paleotopography (House et al. 1998) and its evolution over time (Braun 2002).

Detrital Thermochronology

Another approach to understanding orogenic denudational histories uses cooling ages of detrital minerals eroded from exhumed bedrock and preserved in sediment or sedimentary rocks (e.g., Cerveny et al. 1988, Copeland & Harrison 1990, Brandon & Vance 1992, White et al. 2002). Geochronology of detrital minerals has a long history, especially U/Pb dating of detrital zircons to constrain provenance and ages of sedimentary rocks whose sources are unknown. Beyond provenance, however, U/Pb crystallization ages are often of little use for understanding orogenic erosional histories. The vast majority of zircons eroded from the Himalayas, for example, have zircon U/Pb ages older than 500 Ma, reflecting ancient magmatic or metamorphic events unrelated to the Cenozoic Himalayan orogen. In contrast, most of the (U-Th)/He cooling ages on these same zircons are younger than 4 Ma (Campbell et al. 2005), reflecting cooling associated with rapid exhumation from ZHe closure depths. Thus, thermal history information from thermochronology of detrital minerals is necessary for understanding the erosional history of orogens. Approaches for obtaining both crystallization and cooling ages by combined single-grain U/Pb and (U-Th)/He ages in detrital zircons have recently offered new insights to provenance and exhumation histories in detrital studies (Rahl et al. 2003, Campbell et al. 2005, Reiners et al. 2005a).

Detrital thermochronology offers at least two advantages over bedrock approaches. One is that detrital cooling ages in sedimentary rocks often preserve a much longer record of exhumation than can be obtained from exposed bedrock within the orogen of interest. Bernet et al. (2001), for example, used FT ages of zircons in middle Miocene to Recent sediments to demonstrate exhumational steady state of the European Alps over this time interval. A second advantage is that rivers provide a convenient means of sampling over a large area, especially where access to bedrock exposures is difficult. A single well-mixed fluvial sediment sample may contain detrital contributions from nearly every part of a drainage. Provided analytical methods allow for sufficiently high sample-throughput, large numbers of individual grains can be analyzed to determine cooling age distributions representative of each drainage, which can be analyzed in several ways, as described below.

Lag Time

One goal in detrital thermochronology is determination of lag time, defined as the difference between the cooling age and depositional age for a detrital mineral (Garver et al. 1999). Detrital minerals can be recycled through multiple erosional and depositional cycles (Sherlock 2001, Reiners et al. 2005a). Even so, there is good evidence that in active orogens, the time between erosion and deposition is likely very short (<1 Myr) when compared to the amount of time associated with exhumation (Copeland & Harrison 1990, Heller et al. 1992, Bernet et al. 2004, Stewart & Brandon 2004). If cooling occurred by erosion, then the lag time can be used to estimate erosion rates in the source region of the sediment. The relationships in **Figure 4** could be used for cases where lag times were steady or changed slowly with time (quasi-steady). Evolution of lag time through a stratigraphic sequence can

then be interpreted as evolution of spatially averaged exhumation rates in the source. Decreasing lag times upsection would represent increasing exhumation rates through time, consistent with a constructional phase of mountain building, whereas increasing lag times would suggest a decaying mountain range, and an invariant lag time through the section would be consistent with exhumational steady state—an important conclusion for tectonogeomorphic studies. A potential complication to lag time interpretations of this type includes the possibility for exhumation and cooling ages produced by tectonic, rather than erosional, exhumation. Shallow magmatism and volcanism will also complicate the situation. In this case, the lag time is no longer related to the rate of exhumation. The success of detrital thermochronology studies in the Alps and the Himalaya has been because these areas have seen little shallow magmatism or volcanism throughout the Cenozoic.

Lag times can be interpreted from detrital cooling age distributions in several ways, depending on their form. Detrital samples commonly contain a diverse mix of grain ages and statistical methods are needed to resolve components or peaks in the age distribution (Brandon 1992, 1996, 2005, as summarized in Ehlers et al. 2005). Bernet et al. (2001) used this approach to resolve two main age peaks in FT ages of detrital zircons sourced from the Alps in seven samples ranging in depositional age from modern to 15 Ma. The youngest (P1) peak composed 15%–50% of the zircons in each sample, and represented a constant lag time of 8 Myr. They interpreted this to represent exhumational steady state of the Alps since at least 15 Ma, a conclusion that appears to conflict with other studies that have argued for increased erosion rates in the last 2–4 Myr owing to climate change (Molnar 2004, Cederbom et al. 2004).

Cooling Age Distributions of Detrital Minerals

More information on the erosional dynamics of a source region is contained in the distribution of cooling ages from a sample. Stock & Montgomery (1996) outlined a method for constraining paleorelief in orogenic drainages by considering the observed range of cooling ages and an estimate of the AER in the drainage. Essentially, the range of ages observed, a_r, should be the product of the topographic relief R, and the rate of change of age with elevation da/dz. As discussed above, the inverse of da/dz can, subject to assumptions, be an estimate of erosion rate. Using this approach, Hodges and coworkers (Brewer et al. 2003, Hodges et al. 2005, Ruhl & Hodges 2005) have turned the relationship around to estimate time-averaged erosion rates in drainages with known or assumed relief. As an example, Ruhl & Hodges (2005) analyzed 111 single-grain $^{40}Ar/^{39}Ar$ laser fusion ages of detrital muscovite from the Nyadi drainage in central Nepal, finding a 13.4-Myr age range. Dividing this by the ~6.2-km topographic relief in the drainage yields an estimated erosion rate of ~0.5 km Myr^{-1}, although the authors state that a more rigorous analytical screening of the data reduces the age range to 8.3 Myr and an estimated erosion rate of 0.75 km Myr^{-1}. As stated above, this is a time-averaged erosion rate, which is essentially based on the mean age of the observed age distribution. The abundance of very young ages in the distribution indicate that exhumation rates increased significantly sometime after ~2–11 Ma. Significant changes in erosion rates over time can also be

tested by comparing the form of the probability density plot for the observed cooling ages with that predicted by combining the drainage's hypsometric curve with the observed age-elevation trend, if known (Hodges et al. 2005). If significant mismatches occur, alternative synthetic age probability density functions with spatially varying uplift/sediment-source functions or temporally varying erosion rates could be fit to the observed one to infer detailed variations in erosion rates in space and time. For example, if a single AER could be demonstrated or assumed for a source region, differences between the observed age probability density plot and that predicted for a spatially constant erosion rate could constrain the spatial distribution of erosion and, potentially, the changing relief of the source region. Alternatively, if the spatial distribution of erosion could be demonstrated or assumed to be constant in a source region, the hypsometry and the age probability density functions could be combined to yield a synthetic AER for the region that shows changes in erosion rate with time.

Interdrainage variations in cooling age distributions of detrital minerals have also been used to elucidate first-order tectonic features of active mountain ranges. Bedrock sampling or observations in many regions is impossible due to extreme relief or dense vegetation. In such cases, detrital ages may provide the only means to map geologic structures and their controls on erosion rates. Wobus et al. (2003) observed a shift from Paleozoic-Mesoproterozoic to Miocene and younger muscovite $^{40}Ar/^{39}Ar$ cooling ages across a physiographic transition in the Himalayan foothills where no structures were previously mapped. The transition also marks a dramatic shift in cosmogenic nuclide concentrations in fluvial sediment, supporting the inference of a major, active, out-of-sequence fault in this location (Wobus et al. 2005). The coincidence of a major change in precipitation also at this location led these authors to suggest a possible positive feedback between precipitation, erosion, and rock uplift here.

SPATIAL PATTERNS OF COOLING AGES IN OROGENS

Whereas bedrock vertical transects of cooling ages constrain temporal changes in exhumation rates, sampling over broad areas in an orogen constrains spatial patterns of time-averaged exhumation rates. This can be useful for finding active or formerly active structures, or for elucidating the larger-scale kinematics of the orogenic system.

As described above, several studies have used spatial patterns of thermochronometric ages to identify previously unknown faults or to demonstrate large differences in uplift and exhumation rates across previously known faults. As another example, Spotila et al. (2001) used apatite (U-Th)/He dating across strands of the San Andreas Fault Zone in southern California to show that a narrow crustal sliver in this transpressional zone had experienced ~3–6 km of exhumation since 1.8 Ma.

Other studies have focused on constraining the timing and rates of slip along normal faults, using the fact that footwalls are progressively tectonically exhumed perpendicular to fault strike. Many studies have focused specifically on these issues in the classic core complexes in the Basin and Range of the western United States (Foster et al. 1991, 1993; John & Foster 1993; Howard & Foster 1996; Scott et al. 1998; Foster & John 1999; Brady 2002; Carter et al. 2004). These studies find generally consistent slip rates of ~2–7 mm/year. Estimating fault slip rates, however, can be complicated

by the combined effects of fault geometry, advection of isotherms in the footwall, and syn- or postfaulting erosion and rotation of the footwall (Ketcham 1996, Ring et al. 1999a, Ehlers et al. 2001, Grasemann & Dunkl 2003).

Convergent Orogens

Spatial patterns of thermochronometric ages in convergent orogens are typically interpreted differently than in extensional settings. In some cases, cooling age variations can be related to individual structures and related to the kinematics of discrete faults or folds. At some scales, however, low-T thermochronometers are more usefully interpreted in the context of overall movement of material through an orogenic system. In this context, a few large structures, such as orogen-bounding thrust faults, may set the boundary conditions for deformation within the orogen, but individual structures are ephemeral, and the particle paths of materials moving through an orogen can appear continuous at the scale of the orogen.

This perspective has been aided by the critical wedge model. Critical wedge theory was originally developed to describe the growth, form, and deformation within submarine accretionary complexes or thin-skinned fold-and-thrust belts, where crustal thickening is caused by horizontal accretion of rock directly above a subducting plate (Chapple 1978; Davis et al. 1983; Dahlen 1984, 1990). The essential principles and processes governing critical wedge behavior have since been generalized to a wide range of orogens. The fundamental feature of the theory is that the overall form of the orogen and the deformation within it are governed by the interaction of gravitational forces set by the topographic form of the wedge, the basal shear stress on the decollement beneath it, and the fact that every point within the deforming wedge is at the point of plastic failure. The criticality of a critical wedge arises from the self-adjustment of surface slopes to critical angles so that gravitational forces maintain every point in the interior of the wedge at plastic failure.

Patterns of cooling ages within orogenic wedges provide a useful way to characterize tectonic features, such as the distribution and magnitude of accretionary and erosional fluxes. One of the best-studied orogenic wedges is the emergent part of the forearc wedge of the Cascadia subduction zone–the Olympic Mountains, in western Washington State (**Figure 7**). Brandon et al. (1998) reported AFT ages across the Olympics wedge, and used an erosion-rate dependent crustal thermal model to invert

Figure 7

Wedgeology of the Olympic Mountains, Washington State. Upper panel: Digital elevation model of the Olympic Mountains and Cascadia region, showing location of A-A′ transect shown in bottom panel. Middle panel: Schematic cross-section from west to east through the range, illustrating the geodynamic setting and presumed particle paths through the wedge (after Batt et al. 2001). Lower panel: Erosion rates inferred from strath terraces (*red* and *light blue symbols*) and AFT ages (*yellow symbols*), the latter using the methods summarized in this review (after Brandon et al. 1998). Precipitation (*blue line*) is the mean annual rate for 30 years, from Spatial Climate Analysis Service, Oregon State University (**http://www.ocs.oregonstate.edu/prism/**).

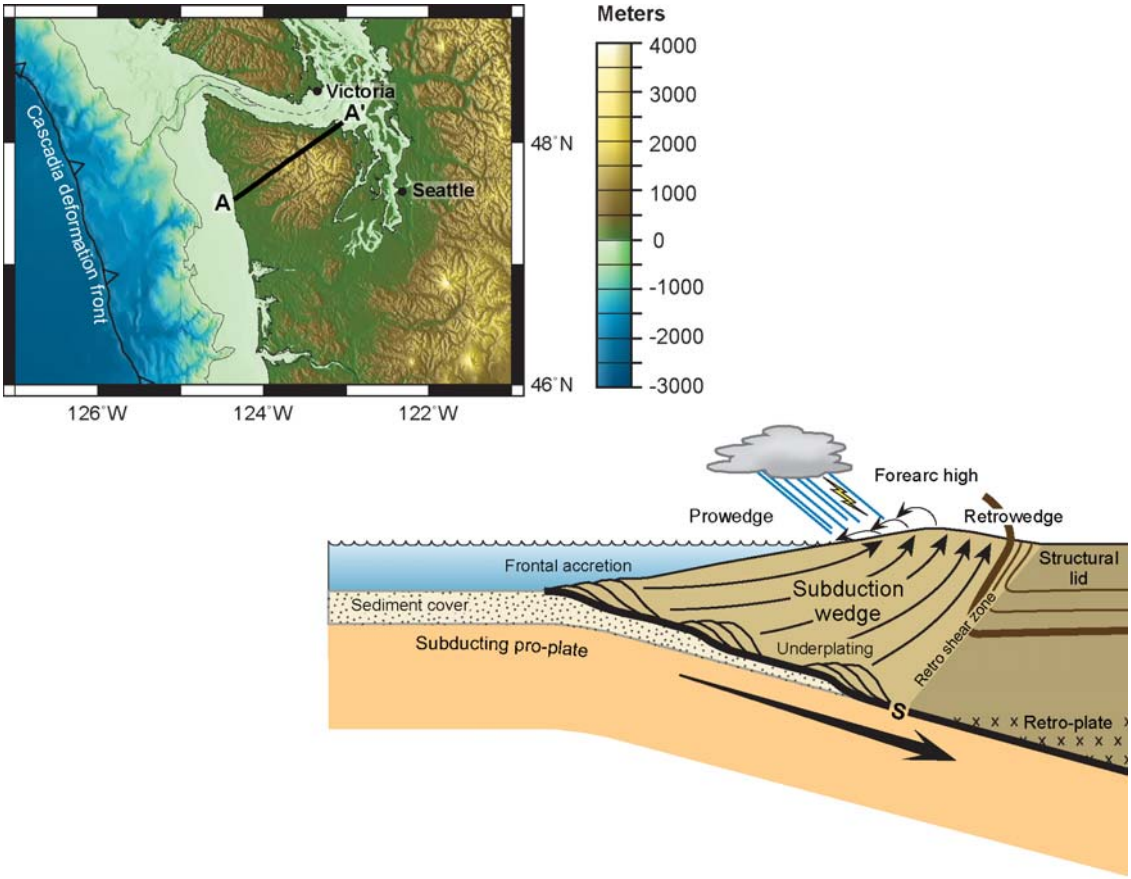

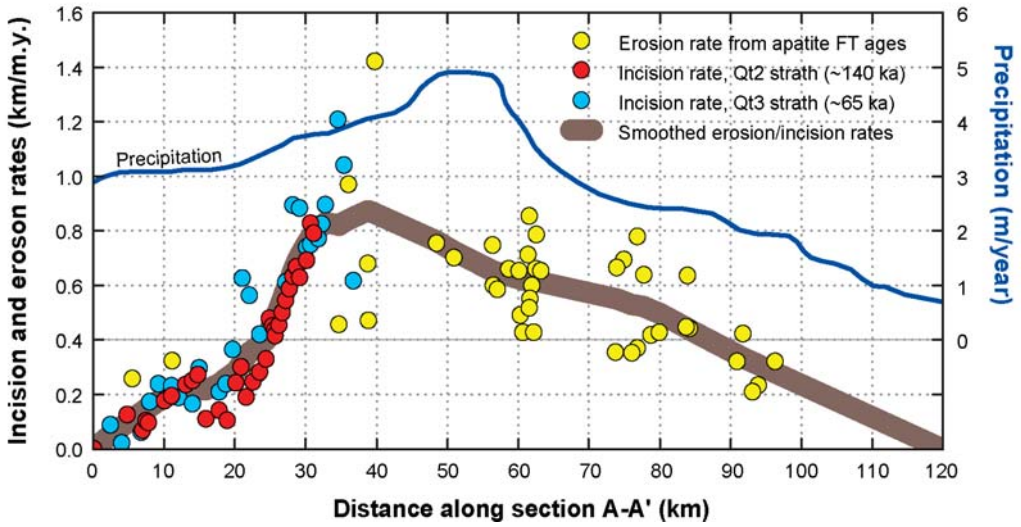

these ages for time-averaged erosion rates. The results (**Figure 7**) show a maximum erosion rate of about 1 km Myr^{-1} on the windward side of the range, which decreases to zero across the range, in the direction of plate convergence. These erosion rates, as well as their spatial variation, which represent estimates averaged over timescales of about 7 to 15 Myr, are remarkably consistent with fluvial incision rates determined from abandoned river channels, about 65 and 140 ka in age, that are now preserved as uplifted remnants above the modern river channel (Pazzaglia & Brandon 2001). This result indicates that erosion rates at the regional scale are similar to river incision rates at the local scale. This observation, and others, indicate that the erosion and uplift are in balance and that the long-wavelength topography of the Olympics has been steady since ~15 Ma (Brandon et al. 1998, Pazzaglia & Brandon 2001, Batt et al. 2001).

Further study of the Olympic wedge by Batt et al. (2001) showed that bedrock ages of the ZFT, AFT, and AHe systems, with their strongly contrasting thermal sensitivities, showed nested concentric resetting zones. Using a two-dimensional kinematic and thermal model of the range as a steady-state wedge, they used the spatial pattern of ages for each system to model two-dimensional particle paths within the wedge, subject to two free parameters and constrained by best-fit results to all three thermochronometric systems. The first free parameter represented the relative flux of material into the wedge, whether by frontal accretion at the toe of the wedge or by underplating deep beneath it. The second free parameter was the maximum erosion rate at the surface of the wedge. The erosion rate profile was assumed to have the form shown in the lower panel of **Figure 7**, but the intensity of the erosion was allowed to vary according to the maximum erosion rate parameter. The steady-state requirement indicated that local rates for rock uplift and erosion were equal. The best-fit solutions demonstrated that accretion occurs primarily at the front of the wedge and the maximum erosion rate parameter is 0.9–1.0 km Myr^{-1} , Frontal accretion results in a significant gradient in horizontal velocities across the Olympics, equal to a decrease of about 3 mm $year^{-1}$ toward the northwest along the A-A' profile in **Figure 7** (Pazzagalia & Brandon 2001).

Horizontal transport explains why regions of many wedges show thermochronologic evidence for high exhumation rates for long periods of time, but expose only weakly metamorphosed rocks. In other words, the vertical component of exhumation for many rocks in these settings comprises only a minor part of the total path through the wedge. This is important because it means that the thermal history experienced by rocks in the orogen may be strongly influenced by paths where the horizontal transport is much greater than the vertical transport (Batt & Brandon 2002). Rocks that never exceeded PRZ temperatures of a given thermochronologic system during residence in the orogen may have young ages after exhumation. These ages may appear reset, but the effective closure temperature concept would not apply since the samples did not pass entirely through the PRZ.

Climate-Tectonic Feedbacks

The critical wedge model has important implications for the relationships between erosion, tectonics, and climate. An important feature of critical wedge theory is that

the links between gravitational forces, shear stress, and internal plastic failure set the form of a convergent wedge so that the cross-section of the wedge will grow in a self-similar fashion. The balance between erosional and accretionary fluxes determine whether the wedge will grow, shrink, or remain constant in size. Importantly, this means that the wedge must deform internally to match accretionary fluxes with erosional fluxes while maintaining its critical taper form.

Erosion rates may be localized within an orogen by focused fluvial erosion, which has been proposed as a mechanism for strong localization of deformation and rock uplift (Molnar & England 1990, Zeitler et al. 2001, Koons et al. 2002, Simpson 2004). On a broader scale, variations in precipitation are likely to cause variations in erosion rates, which suggests a potentially important feedback between climate and tectonics at the orogen scale (Willett 1999). This erosional feedback, as well as other fundamental features of the critical wedge model, are expected to hold for a much wider range of convergent orogenic settings and scales than the submarine accretionary complexes or fold-and-thrust belts for which they were originally developed (Jamieson & Beaumont 1988, Beaumont et al. 1992, Willett et al. 1993, Willett & Beaumont 1994, Royden 1996, Koons et al. 2003). In other words, a generalized concept of critical topography can probably be applied to most if not all convergent orogens (Willett 1999).

Thermochronologic evidence for correlations between modern precipitation and long-term erosion rates within orogens has been presented for several orogens, including Irian Jaya, Indonesia (Weiland & Cloos 1996), the Olympic Peninsula (Willett 1999), the central Washington Cascades (Reiners et al. 2003a), and the Himalayan front (Wobus et al. 2003). Common to all these examples is a pronounced offset of the maximum height of the topography with those for the erosion rate and precipitation. In all cases, faster erosion and greater precipitation are found on the windward side of the orogen. In the Himalayan case, Wobus et al. (2005) inferred that an individual out-of-sequence thrust is responsible for a sharp change in erosion rate over a short distance, but in other cases, the activity of individual structures is not apparent.

The Cascades transect shows a relatively smooth gradient in exhumation rates (as inferred from AHe ages) across the range, although rates are relatively scattered in the region with the highest values (**Figure 8**). The scatter may result from transients in topography, geothermal gradients, or the erosion rates themselves. In this part of the orogen, the Cascades comprise dominantly uplifted crystalline basement. Although one might worry that transient magmatic cooling may have affected some of the cooling ages, we note that nearly all apatite He ages are significantly younger than intrusion ages, and so likely reflect erosional exhumation.

The unusual uplifted arc setting of the central and northern Cascades make it difficult to interpret the kinematic origin or dynamic significance of the cross-range AHe age pattern, and its apparent coupling with modern precipitation rate, at least in terms of a classical critical wedge model. The lack of sharp breaks in the pattern is not easily reconcilable with uplift by slip on discrete faults. Seismicity shows no evidence of active discrete structures in the Cascade Range. Nevertheless, close correspondence between the patterns of precipitation and erosion rate is striking. One speculative possibility for this correlation is that uplift and exhumation in the Washington

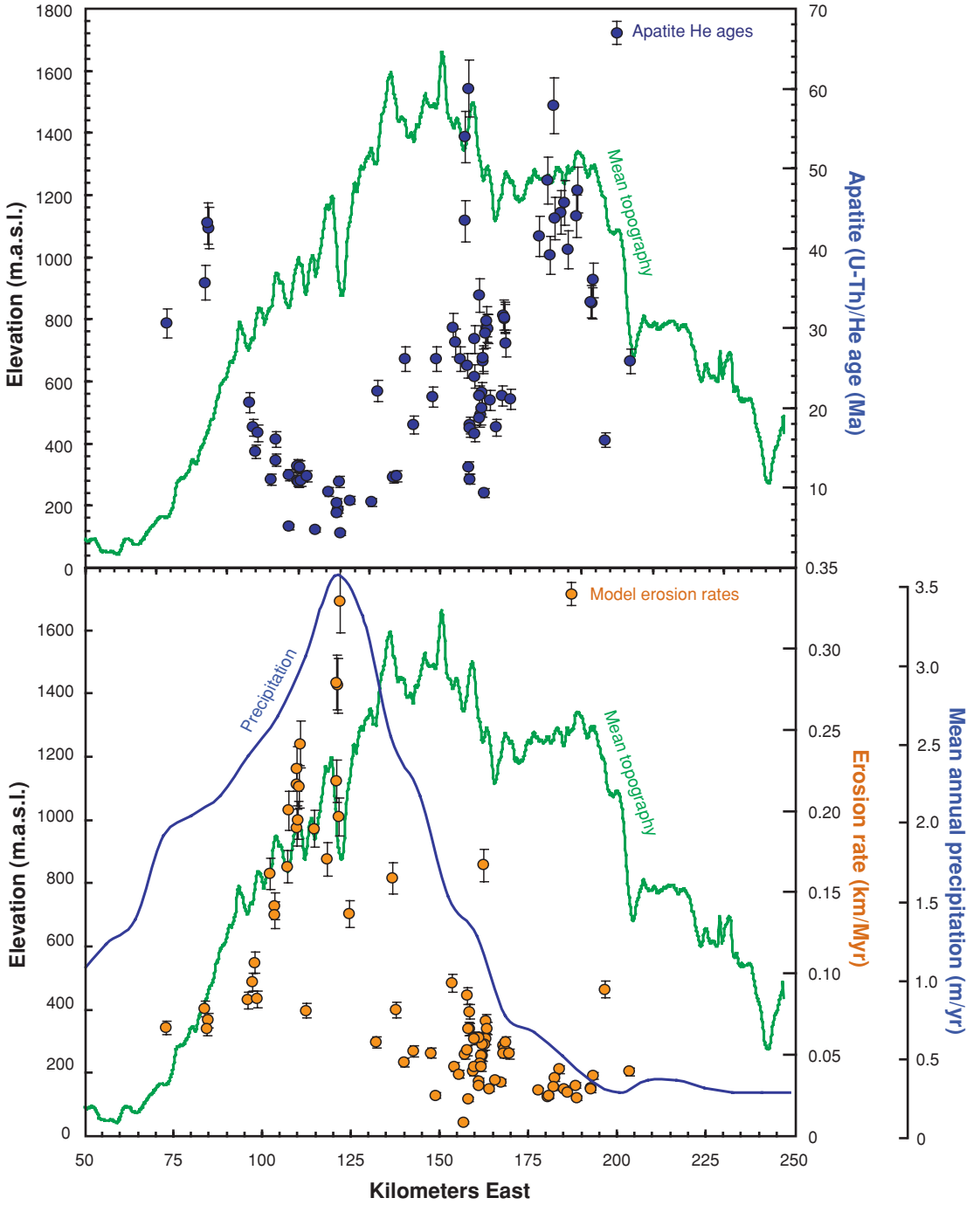

Cascades may be due to coupling between erosion and magmatic intrusions at depth, fed by the active arc. Although there is no dynamic model for arc-related orogens analogous to the critical wedge model, it is possible that strain and exhumation in such a setting may occur by mobilization of melt-weakened crust or plutons, rather than by faults, so that weakened crust or magmas are preferentially emplaced beneath regions of high erosional exhumation. This may be similar to the models of lateral extrusion of melt-weakened crust owing to high precipitation at the edge of the Tibetan plateau (Beaumont et al. 1992, 2001; Hodges et al. 2004), and the model of channelized flow and crustal aneurysm due to focused fluvial erosion at the syntaxes of the Himalaya (Zeitler et al. 2001, Koons 2002).

Glacial Erosion

The rugged high-relief topography characteristic of many modern mountain ranges owes much of its development to Quaternary glacial erosion. Dramatic topographic features provide clear qualitative evidence of the erosive potential of glaciers (e.g., Montgomery 2002), and measurements of sediment fluxes from glacially eroded catchments have been used to argue that glacial erosion rates are one to two orders of magnitude higher than fluvial erosion rates (Hallet et al. 1996). In addition to increasing topographic relief by valley deepening, some studies have suggested that glaciers may also increase peak heights, via isostatically induced uplift (Molnar & England 1990, Small & Anderson 1998), although this remains controversial (Whipple et al. 1999, Tomkin & Braun 2002). On both global and regional scales, the remarkable correspondence between regional peak heights and equilibrium-line altitudes (ELAs) of glaciers suggests that glaciers may also act as buzz saws that limit maximum elevations (Porter 1981, Broecker & Denton 1990, Brozovic et al. 1997).

ELA: equilibrium-line altitudes

If the rapid pace of glacial erosion suggested by short-term sediment yields persist over million-year timescales, and if glaciers do act as regionally important topographic buzz saws, they should produce clear thermochronologic signals in bedrock or detrital cooling-age patterns. Thermochronologic assessments of the general importance of glacial erosion thus far, however, show mixed results. Using He dating, Spotila et al.

Figure 8

Top panel: Mean elevation of topography in a 50-km wide east-west swath through the Washington Cascades at about the latitude of Seattle (*green line*), with apatite (U-Th)/He ages of samples within the swath. AHe ages are mean ages of two to six single-grain analyses per sample (only one point per sample is shown); 6% (2 RSE) error bars represent typical reproducibility among replicate analyses. AHe ages show an overall U-shaped pattern with distance, varying from approximately 4.0 to 60 Ma across the range, with a minimum about halfway up the west flank of the range. This figure shows new data not shown in a similar figure in Reiners et al. (2003a). Bottom panel: Erosion rates estimated for each sample using the steady-state method illustrated in **Figure 4**. Also shown is the mean annual precipitation rate over a ~30-year period (Spatial Climate Analysis Service, Oregon State University, **http://www.ocs.oregonstate.edu/prism/**). Both precipitation and erosion show an order of magnitude variation, with maxima that are displaced towards the windward side of the range.

(2004) showed that long-term (10^6 years) erosion rates in the Chugach Mountains are well correlated with the distribution of modern glaciers. Furthermore, accretionary and erosional fluxes appear to be in balance at the scale of orogen, but these rates are no greater than ~3 mm/year, which is an order of magnitude lower than short-term measurements of glacial erosion (Hallet et al. 1996). T.A. Ehlers, K.A Farley, M.E. Rusmore & G.J. Woodsworth (manuscript submitted) also found long-term (<1–10 Myr) rates of less than 1 mm/year in the highly glaciated landscape of the Coast Mountains of British Columbia. However, Ehlers et al. (manuscript submitted) also used regional patterns of AHe ages to suggest that topographic relief has increased by 1.6–2.2 km and valleys have widened dramatically since 7.5 Ma. Using $^4He/^3He$ thermochronometry on some of the same samples, Shuster et al. (2005) concluded that at least 2 km of valley incision occurred, beginning at 1.8 ± 0.2 Ma, requiring local erosion rates over this duration of at least 5 km Myr^{-1}. Although this rate is far lower than short-term sediment yield estimates of Hallet et al. (1996), these results suggest that, at least locally, glacial erosion rates can be much higher than regional erosion rates. However, when measured as valley-bottom incision rates, fluvial erosion rates can also be quite high (e.g., Burbank et al. 1996, Lavé & Avouac 2001). This points out the difficulty in assigning the importance of one erosional mechanism over another when erosion rates can vary by orders of magnitude over different spatial and temporal scales in a single orogen.

A more general question of the significance of glacial erosion is how it might affect the tectonic behavior of mountain ranges. As described above, numerous studies have highlighted the important role erosion may play in limiting the elevation and width of orogens, in the context of a critical wedge (Dahlen & Barr 1989, Willett 1999, Hilley & Strecker 2004, Whipple & Meade 2004). If glaciation can indeed act as a topographic buzz saw, then the onset of glacial conditions and lowering of the ELA should rapidly decrease the elevation of an orogen. This erosion will induce a rock uplift response, but the magnitude and distribution of the response will depend on the tectonic conditions of the range. If the range is tectonically inactive, uplift will be limited to isostatic rebound, and the change in erosion rate for areas intersecting the ELA will be inversely proportional to the isostatic compensation ratio (~0.2; Pazzaglia & Brandon 1996), flexural effects notwithstanding. If the range behaves as a critical orogenic wedge (see Sidebar), however, the consequences are more interesting. The descending ELA will intersect and rapidly erode the crest of the wedge, decreasing its elevation. Maintenance of critical taper dictates that the wedge will respond not only by increasing uplift rates in this portion of the wedge, but also by decreasing the overall wedge width, which requires even faster erosion. Numerical simulations of both passive and active wedge scenarios for typical wedge parameters, using ELA lowering rates estimated for Quaternary glacial cycles (Broecker & Denton 1990), predict changes in erosion rates of about 0.5 to 2 km Myr^{-1} (J.H. Tomkin & M.T. Brandon, manuscript submitted), which should be easily detectable using standard He or FT dating approaches. Testing for the orogenic response to alpine glaciation in such a scenario could be done by examining both timing and magnitudes of erosional rate changes along strike of ELA-lowering gradients such as latitude.

CRITICAL OROGENIC WEDGE

The critical orogenic wedge is a deforming wedge of crustal material that forms where plates converge. The wedge is bounded by a basal thrust or decollement (**Figure 7**) that allows one plate to subduct beneath another. Some material is transferred by accretion from the subducting plate to the overriding plate, causing the wedge to deform and grow with time. The wedge will deform internally until it reaches a critical taper in which the wedge is blunt enough and strong enough to overcome the resistance to slip on the decollement. Further accretion at the front of the wedge or erosion at the top of the wedge will reduce the taper and the integrated strength of the wedge. The wedge will respond by deforming and thicken internally until it recovers a blunter and stronger taper. This feedback causes an orogenic wedge to remain close to its critical taper when perturbed by frontal accretion and erosion. The critical wedge model predicts that spatially focused erosion should result in spatially focused deformation and rock uplift.

SUMMARY POINTS

1. Erosion denudes orogens and exhumes rocks. Spatial patterns of erosion in orogens can influence tectonic deformation and uplift. For example, focused orographic precipitation can cause focused erosion, which may lead to focused tectonic strain. Thermochronology can constrain spatial-temporal patterns of erosion in orogens on $\sim 10^5$–10^7 year timescales, commensurate with cycles of orogenic growth and decay, and the response time for possible feedbacks between climate and tectonics.
2. The most commonly used low- to intermediate-temperature thermochronometers use (U-Th)/He and fission-track systems in U-Th-bearing minerals, most commonly apatite and zircon, and the $^{40}Ar/^{39}Ar$ (and K/Ar) systems in feldspar, micas, and hornblende. Diffusion of ^4He and ^{40}Ar and annealing of fission tracks are well represented by thermally activated diffusion, which allows quantitative predictions of the thermal sensitivities of the thermochronometers. The partial retention zone (PRZ) describes the temperature range where thermochronometers are able to only partially retain the products of radioactive decay (^4He, fission tracks, ^{40}Ar). The loss-only PRZ temperatures range from $\sim 20^\circ C$–$60^\circ C$ for the apatite He system to $\sim 400^\circ C$–$525^\circ C$ for the hornblende $^{40}Ar/^{39}Ar$ system and correspond to crustal depths of ~ 1 km to several tens of kilometers.
3. For monotonic cooling histories, the thermal sensitivity of each system can be represented by an effective closure temperature, which is the temperature of the mineral at the measured thermochronometric age (the cooling age)

for steady monotonic cooling. Closure temperatures for commonly used thermochronometers range from about 65°C to 550°C for the apatite He and hornblende Ar systems, respectively, assuming typical orogenic cooling rates.

4. Given a crustal thermal model, which can be adapted to specific orogenic settings, thermochronometric cooling ages can be uniquely related to an erosion rate, assuming this rate has been steady prior to and after closure of the system. Changes in erosion rate can cause transient movement of isotherms relative to Earth's surface, which can invalidate this estimate. Thermochronometers with low closure temperatures are able to recover more rapidly from transients and thus are more likely to follow the steady-state solution.
5. Changes in erosion rates with time can be constrained from measurements of multiple cooling ages from the same rock, provided transient thermal effects are considered, or from the distribution of cooling ages of a single system with elevation in vertical transects. Age-elevation relationships in a vertical transect can provide two estimates of erosion rates. The first estimate is given by the slope of the age-elevation profile and is representative of the time interval represented by the cooling ages. The second estimate is representative of the average erosion rate over the time interval from the cooling age at the mean elevation of the profile to present. Key assumptions for the vertical transect method are that the closure isotherm is relatively flat under the study area and remained at a constant depth during the time interval represented by the cooling ages in the profile.
6. Detrital thermochronology uses the distribution of grain ages from a single sample of sediment or sedimentary rock to constrain the exhumational history of the source region of the sediment. Lag time represents the amount of time that elapsed between passage of the dated grain through the closure depth for the thermochronometer and deposition of the sediment. Changes in lag times in sediments shed from the same orogen over time can constrain the growth and decay of the orogen. Detrital grain age distributions can also be used to constrain paleorelief, and determine spatial or temporal variations in exhumation rates.
7. Spatial patterns of bedrock cooling ages in orogens can be used to map out variations in erosion rates and their relationships with kinematic models for material flow through orogenic wedges, climatic variations, or structural or geomorphic features. In some cases, spatial patterns of thermochronometrically determined erosion rates are strikingly similar to those determined from much shorter-term geomorphic features, or to modern patterns of precipitation.

FUTURE DIRECTIONS

1. Many of the recent advances in the methods, interpretations, and applications of thermochronology have been motivated by growing interest in the connections between tectonic, geomorphic, and climatic processes. Partly as a result, considerable interest has focused on thermochronometers sensitive to low temperatures, such as apatite FT and He. One emerging method with great potential to extend the sensitivity to even lower temperatures, as well as estimate continuous time-temperature paths during exhumation, is $^{4}He/^{3}He$ thermochronometry (Shuster et al. 2003, 2005; Shuster & Farley 2003, 2005). This method measures intracrystalline ^{4}He distributions to resolve the cooling path from ~80°C to the surface. Intracrystalline ^{4}He variations may also be measured in other ways (such as in situ laser ablation), opening up the possibility of routinely estimating cooling paths rather than a single closure temperature.
2. As is well-known from detrital studies, many problems in orogenic systems require thermochronologic data from large areas involving many samples and individual grain ages. This approach allows one to image broad-scale tectonic or erosional patterns and simply reduce statistical uncertainty. A challenge for thermochronology is to find ways to increase the number of grains that can be dated while maintaining good precision. The availability of synoptic datasets for large areas or distributions of hundreds of detrital grain ages from single catchments will lead to new discoveries in how surface processes affect the orogenic systems.
3. There is growing interest in combining thermochronology with other approaches to study orogenic evolution. Examples include using combined thermochronologic and cosmogenic methods with river chemistry and climate data to understand the interrelation between physical and chemical erosion at different timescales.
4. In general, there is a need for a more robust understanding of the interaction of tectonics, erosion, and climate in orogenic systems. Although theoretical approaches suggest important linkages between them, actual evidence from thermochronologic or other approaches is often ambiguous. Important progress will come from well-posed natural experiments that will allow a close examination of climate, surface processes, and tectonics at different time- and length-scales.

ACKNOWLEDGMENTS

This work was supported in part by NSF grant EAR-0236965 to PWR and the RETREAT project, funded by grant EAR-0208652 from the NSF Continental Dynamics program to MTB and PWR.

LITERATURE CITED

Armstrong RL. 1966. K-Ar dating of plutonic and volcanic rocks in orogenic belts. In *Potassium-Argon Dating*, ed. OA Schaeffer, J Zähringer, pp. 117–33. Berlin: Springer–Verlag

Baldwin SL, Lister GS. 1998. Thermochronology of the South Cyclades Shear Zone, Ios, Greece: effects of ductile shear in the argon partial retention zone. *J. Geophys. Res.* 103:7315–36

Barbarand J, Carter A, Wood I, Hurford T. 2003. Compositional and structural control of fission-track annealing in apatite. *Chem. Geol.* 198:107–37

Batt GE, Brandon MT. 2002. Lateral thinking: 2-D interpretation of thermochronology in convergent orogenic settings. *Tectonophysics* 349:185–201

Batt GE, Brandon MT, Farley KA, Roden-Tice M. 2001. Tectonic synthesis of the Olympic Mountains segment of the Cascadia wedge, using two-dimensional thermal and kinematic modeling of thermochronological ages. *J. Geophys. Res.* 106:26731–46

Baxter EF. 2003. Quantification of the factors controlling the presence of excess ^{40}Ar or ^{4}He. *Earth Planet. Sci. Lett.* 216:619–634

Beaumont C, Fullsack P, Hamilton J. 1992. Erosional control of active compressional orogens. In *Thrust Tectonics*, ed. KR McClay, pp. 1–18. London: Chapman and Hall

Beaumont C, Jamieson RA, Nguyen MH, Lee B. 2001. Himalayan tectonics explained by extrusion of a low-viscosity crustal channel coupled to focused surface denudation. *Nature* 441:738–32

Bernet M, Brandon MT, Garver JI, Molitor BR. 2004. Downstream changes in Alpine detrital zircon fission-track ages of the Rhône and Rhine Rivers. *J. Sed. Res.* 74:82–94

Bernet M, Zattin M, Garver JI, Brandon MT, Vance JA. 2001. Steady state exhumation of the European Alps. *Geology* 29:35–38

Bierman P, Steig EJ. 1996. Estimating rates of denudation using cosmogenic isotope abundances in sediment. *Earth Surf. Proc. Landf.* 21:125–39

Brady RJ. 2002. Very high slip rates on continental extensional faults: new evidence from (U-Th)/He thermochronometry of the Buckskin Mountains, Arizona. *Earth Planet. Sci. Lett.* 197:95–104

Brandon MT. 1992. Decomposition of fission-track grain-age distributions. *Am. J. Sci.* 292:535–64

Brandon MT. 1996. Probability density plots for fission-track grain age distributions. *Radiation Meas.* 26:663–76

Brandon MT. 2002. Decomposition of mixed grain-age distributions using BINOMFIT. *On Track* 24:13–18

Brandon MT, Roden-Tice MK, Garver JI. 1998. Late Cenozoic exhumation of the Cascadia accretionary wedge in the Olympic Mountains, Northwest Washington State. *Geol. Soc. Am. Bull.* 110:985–1009

Brandon MT, Vance JA. 1992. Tectonic evolution of the Cenozoic Olympic Subduction Complex, Washington State, as deduced from fission-track ages for detrital zircons. *Am. J. Sci.* 292:565–636

Braun J. 2002. Quantifying the effect of recent relief changes on age-elevation relationships. *Earth Planet. Sci. Lett.* 200:331–43

Brewer ID, Burbank DW, Hodges KV. 2003. Modelling detrital cooling-age populations: insights from two Himalayan catchments. *Basin Res.* 15:305–20

Brewer ID, Burbank DW, Hodges KV. 2005. Downstream development of a detrital cooling-age signal: insights from $^{40}Ar/^{39}Ar$ muscovite thermochronology in the Nepalese Himalaya. In *GSA Spec. Pap. 398*, *Tectonics*, *Climate*, *and Landscape Evolution*, ed. SD Willet, N Hovius, MT Brandon, DM Fisher. Boulder, CO: Geol. Soc. Am. In press

Brix MR, Stöckhert B, Seidel E, Theye T, Thomson SN, Küster M. 2002. Thermobarometric data from a fossil zircon partial annealing zone in high pressure–low temperature rocks of eastern and central Crete, Greece. *Tectonophysics* 349:309–26

Broecker WS, Denton GH. 1990. The role of ocean-atmosphere reorganizations in glacial cycles. *Quat. Sci. Rev.* 9:305–41

Brown ET, Stallard RF, Larsen MC, Raisbeck GM, Yiou F. 1995. Denudation rates determined from the accumulation of in situ-produced ^{10}Be in the Luquillo Experimental Forest, Puerto Rico. *Earth Planet. Sci. Lett.* 129:193–202

Brozovic N, Burbank DW, Meigs AJ. 1997. Climatic limits on landscape development in the Northwestern Himalaya. *Science* 276:571–74

Burbank DW. 2002. Rates of erosion and their implications for exhumation. *Mineral. Mag.* 66:25–52

Burbank DW, Leland J, Fielding E, Anderson RS, Brozovic N, et al. 1996, Bedrock incision, rock uplift and threshold hillslopes in the northwestern Himalaya. *Nature* 379:505–10

Campbell IH, Reiners PW, Allen CM, Nicolescu S, Upadhyay R. 2005. He-Pb double-dating of detrital zircons from the Ganges and Indus Rivers: implication for quantifying sediment recycling and provenance studies. *Earth Planet. Sci. Lett.* 207:402–32

Carlson WD. 1990. Mechanisms and kinetics of apatite fission-track annealing: *Am. Mineral.* 75:1120–39

Carlson WD, Donelick RA, Ketcham RA. 1999. Variability of apatite fission-track annealing kinetics. I. Experimental results. *Am. Mineral.* 84:1213–23

Carter TJ, Kohn BP, Foster DA, Gleadow AJW. 2004. How the Harcuvar Mountains metamorphic core complex became cool: evidence from apatite (U-Th)/He thermochronometry. *Geology* 32:985–88

Cederbom CE, Sinclair HD, Schlunegger F, Rahn MK. 2004. Climate-induced rebound and exhumation of the European Alps. *Geology* 32:709–12

Cerveny PF, Naeser ND, Zeitler PK, Naeser CW, Johnson NM. 1988. History of uplift and relief of the Himalaya during the past 18 million years: evidence from sandstones of the Siwalik group. In *New Perspectives in Basin Analysis*, ed. KL Kleinspehn, C Paola, pp. 43–61. New York: Springer

Chapple WM. 1978. Mechanics of thin-skinned fold-and-thrust belts. *Geol. Soc. Am. Bull.* 89:1189–98

Copeland P, Harrison MT. 1990. Episodic rapid uplift in the Himalaya revealed by $^{40}Ar/^{39}Ar$ analysis of detrital K-feldspar and muscovite, Bengal fan. *Geology* 18:354–59

Dahlen FA. 1984. Noncohesive critical Coulomb wedges: an exact solution. *J. Geophys. Res.* 89:10125–33

Dahlen FA. 1990. Critical taper model of fold-and-thrust belts and accretionary wedges. *Annu. Rev. Earth Planet. Sci.* 18:55–90

Dahlen FA, Barr TD. 1989. Brittle frictional mountain building 1. Deformation and mechanical energy budget. *J. Geophys. Res.* 94:3906–22

Davis DJ, Suppe J, Dahlen FA. 1983. Mechanics of fold-and-thrust belts and accretionary wedges. *J. Geophys. Res.* 88:1153–72

Dodson MH. 1973. Closure temperature in cooling geochronological and petrological systems *Contrib. Mineral. Petrol.* 40:259–74

Dodson MH. 1976. Kinetic processes and thermal history of slowly cooling solids. *Nature* 259:551–53

Dodson MH. 1979. Theory of cooling ages. In *Lectures in Isotope Geology*, ed. E Jager, JC Hunziker, pp. 194–202. Berlin: Springer-Verlag

Donelick RA. 1986. *Mesozoic-Cenozoic thermal evolution of the Atlin terrane, Whitehorse Trough, and Coast Plutonic Complex from Atlin, British Columbia to Haines as revealed by fission-track geothermometry techniques*. MS thesis. Rensselaer Polytech. Inst., Troy, New York. 167pp.

Donelick RA, Ketcham RA, Carlson WD. 1999. Variability of apatite fission-track annealing kinetics. II. Crystallographic orientation effects. *Am. Mineral.* 84:1224–34

Ehlers TA, Armstrong PA, Chapman DS. 2001. Normal fault regimes and the interpretation of low-temperature thermochronometers. *Phys. Earth Planet. Int.* 126:179–94

Ehlers TA, Chaudhri T, Kumar S, Fuller CW, Willett SD, et al. 2005. Computational tools for low-temperature thermochronometer interpretation. See Reiners & Ehlers 2005, 58:589–622

England P, Molnar P. 1990. Surface uplift, uplift of rocks, and exhumation of rocks. *Geology* 18:1173–77

Ewing RC, Meldrum A, Wang L, Weber WJ, Corrales LR. 2003. Radiation effects in zircon. In *Zircon*, ed. JM Hanchar, PWO Hoskin, pp. 387–425. Washington, DC: Mineral. Soc. Am.

Farley KA. 2000. Helium diffusion from apatite: general behavior as illustrated by Durango fluorapatite. *J. Geophys. Res.* 105:2903–14

Farley KA. 2002. (U-Th)/He dating: techniques, calibrations, and applications. In *Noble Gases in Geochemistry and Cosmochemistry*, *Reviews in Mineralogy and Geochemistry*, 47:819–44. Chantilly, VA: Mineral. Soc. Am., Geochem. Soc.

Farley KA, Rusmore ME, Bogue SW. 2001. Post-10 Ma uplift and exhumation of the northern Coast Mountains, British Columbia. *Geology* 29:99–102

Fechtig H, Kalbitzer S. 1966. The diffusion of argon in potassium-bearing solids. In *Potassium Argon Dating*, ed. OA Schaeffer, J Zähringer, pp. 68–107. New York: Springer-Verlag

Fitzgerald PG, Sorkhabi RB, Redfield TF, Stump E. 1995. Uplift and denudation of the central Alaska Range: a case study in the use of apatite fission track thermochronology to determine absolute uplift parameters. *J. Geophys. Res.* 100:20175–91

Fleischer RL, Price PB, Walker RM. 1965. Effects of temperature, pressure, and ionization of the formation and stability of fission tracks in minerals and glasses. *J. Geophy. Res.* 70:1497–502

Fleischer RL, Price PB, Walker RM. 1975. *Nuclear Tracks in Solids*. Berkely: Univ. Calif. Press. 605pp.

Foland KA. 1994. Argon diffusion in feldspars. In *Feldspars and Their Reactions*, ed. I Parsons, pp.415–47. Amsterdam: Kluwer

Foster DA, Gleadow JW, Reynolds SJ, Fitzgerald PG. 1993. Denudation of metamorphic core complexes and the reconstruction of the transition zone, west central Arizona: constraints from apatite fission track thermochronology. *J. Geophys. Res.* 98:2167–85

Foster DA, John BA. 1999. Quantifying tectonic exhumation in an extensional orogen with thermochronology: examples from the southern Basin and Range Province. See Ring et al. 1999b, 154:343–64

Foster DA, Kohn BP, Gleadow AJW. 1996. *Sphene and zircon fission track closure temperatures revisited; empirical calibrations from $^{40}Ar/^{39}Ar$ diffusion studies of K-feldspar and biotite*. Presented at Int. Workshop on Fission Track Dating, Univ. Gent, Belgium

Foster DA, Miller DS, Miller CF. 1991. Tertiary extension in the Old Woman Mountains area, California: evidence from apatite fission track analysis. *Tectonics* 10:875–86

Galbraith RF, Green PF. 1990. Estimating the component ages in a finite mixture. *Nucl. Tracks Radiation Meas.* 17:197–206

Galbraith RF, Laslett GM. 1993. Statistical models for mixed fission track ages. *Nucl. Tracks Radiation Meas.* 21:459–70

Garver JI, Brandon MT, Roden-Tice MK, Kamp PJJ. 1999. Exhumation history of orogenic highlands determined by detrital fission track thermochronology. See Ring et al. 1999b, 54:283–304

Garver JI, Kamp PJJ. 2002. Integration of zircon color and zircon fission-track zonation patterns in orogenic belts: application to the Southern Alps, New Zealand. *Tectonophysics* 349:203–19

Gleadow AJW, Duddy IR. 1981. A natural long-term track annealing experiment for apatite. *Nucl. Tracks* 5:169–74

Gleadow AJW, Fitzgerald PG. 1987. Uplift history and structure of the Transantarctic Mountains: new evidence from fission track dating of basement apatites in the Dry Valley area, southern Victoria Land. *Earth Planet. Sci. Lett.* 82:1–14

Granger DE, Kirchner JW, Finkel R. 1996. Spatially averaged long-term erosion rates measured from in situ-produced cosmogenic nuclides in alluvial sediment. *J. Geol.* 104:249–57

Grasemann B, Dunkl I. 2003. Effects of the geometry of normal faulting on the near surface heat flow during extension: the example of the Rechnitz Metamorphic Core Complex (Austria). *Mitt. Osterr. Geol. Ges.* 93:87–103

Green PF. 1988. The relationship between track shortening and fission-track age reduction in apatite: combined influences of inherent instability, annealing anisotropy, and length bias and system calibration. *Earth Planet. Sci. Lett.* 89:335–52

Green PF, Duddy IR, Gleadow AJW, Tingate PR. 1985. Fission track annealing in apatite: track length measurements and the form of the Arrhenius plot. *Nucl. Tracks Radiation Meas.* 10:323–28

Green PF, Duddy IR, Laslett GM. 1988. Can fission track annealing in apatite be described by first-order kinetics? *Earth Planet. Sci. Lett.* 87:216–88

Green PF, Duddy IR, Laslett GM, Hegarty KA, Gleadow AJW, Lovering JF. 1989. Thermal annealing of fission tracks in apatite, 4. Quantitative modeling techniques and extension to geological timescales. *Chem. Geol. (Isotope Geosci. Sec.)* 79:155–82

Grove M, Harrison TM. 1996. $^{40}Ar^{*}$ diffusion in Fe-rich biotite. *Am. Mineral.* 81:940–51

Hallet B, Hunter L, Bogen J. 1996. Rates of erosion and sediment evacuation by glaciers: a review of field data and their implications. *Global Planet Change* 12:213–35

Hames WE, Bowring SA. 1994. An empirical evaluation of the argon diffusion geometry in muscovite. *Earth Planet. Sci. Lett.* 124:161–67

Harrison TM. 1981. Diffusion of ^{40}Ar in hornblende. *Contrib. Mineral. Petrol.* 78:324–31

Harrison TM, Armstrong RL, Naeser CW, Harakal JE. 1979. Geochronology and thermal history of the Coast plutonic complex, near Prince Rupert, British Columbia. *Can. J. Earth. Sci.* 16:400–10

Harrison TM, Grove M, Lovera OM, Zeitler PK. 2005. Continuous thermal histories from inversion of thermal profiles. See Reiners & Ehlers 2005, 58:389–409

Heller PL, Renne P, O'Neil JR. 1992. River mixing rate, residence time, and subsidence rates from isotopic indicators: Eocene sandstones of the U.S. Pacific Northwest. *Geology* 20:1095–98

Hickes HJ. 2001. *Apatite and zircon (U-Th)/He thermochronology of the northern Coast Mountains, Southeast Alaska*. MS thesis. Washington State Univ., Pullman, Washington. 42 pp.

Hilley GE, Strecker M. 2004. Steady state erosion of critical Coulomb wedges with applications to Taiwan and the Himalaya. *J. Geophys. Res.* 109:B01411, doi:10.1029/2002JB002284

Hodges KV. 2003. Geochronology and thermochronology in orogenic systems. In *Treatise on Geochemistry*, ed. KK Turekian, HD Holland, pp. 263–92. Oxford, UK: Elsevier

Hodges KV, Ruhl KW, Wobus CW, Pringle MS. 2005. $^{40}Ar/^{39}Ar$ thermochronology of detrital minerals. See Reiners & Ehlers 2005, 58:239–57

Hodges KV, Wobus C, Ruhl K, Schildgen T, Whipple K. 2004. Quaternary deformation, river steepening, and heavy precipitation at the front of the Higher Himalayan ranges. *Earth. Planet Sci. Lett.* 220:379–89

House MA, Wernicke BP, Farley KA. 1998. Dating topography of the Sierra Nevada, California, using apatite (U-Th)/He ages. *Nature* 396:66–69

House MA, Kohn BP, Farley KA, Raza A. 2002. Evaluating thermal history models for the Otway Basin, southeastern Australia, using (U-Th)/He and fission-track data from borehole apatites. *Tectonophysics* 349:277–95

Hovius N, Stark CP, Allen PA. 1997. Sediment flux from a mountain belt derived by landslide mapping. *Geology* 25:231–34

Howard KA, Foster DA. 1996. Thermal and unroofing history of a thick, tilted basin-and-range crustal section in the Tortilla Mountains, Arizona. *J. Geophys. Res.* 101:511–22

Hurford AJ. 1986. Cooling and uplift patterns in the Lepontine Alps, south central Switzerland, and an age of vertical movement on the Insubric fault line. *Contrib. Mineral. Petrol.* 92:413–27

Hurley PM. 1954. The helium age method and the distribution and migration of helium in rocks. In *Nuclear Geology*, ed. H Faul, pp. 301–29. New York: Wiley & Sons

Jamieson RA, Beaumont C. 1988. Orogeny and metamorphism: a model for deformation and P-T-t paths with applications to the central and southern Appalachians. *Tectonics* 7:417–45

John BE, Foster DA. 1993. Structural and thermal constraints on the initiation angle of detachment faulting in the southern Basin and Range: the Chemehuevi Mountains case study. *Geol. Soc. Am. Bull.* 105:1091–108

Kasuya M, Naeser CW. 1988. The effect of α-damage on fission-track annealing in zircon. *Nucl. Tracks Radiation Meas.* 14:477–80

Kelley SP, Arnaud NO, Turner SP. 1994. High-spatial resolution $^{40}Ar/^{39}Ar$ investigations using an ultra-violet laser probe extraction technique. *Geochim. Cosmochim. Acta* 58:3519–25

Kelley SP, Wartho J-A. 2000. Rapid kimberlite ascent and the significance of Ar-Ar Ages in xenolith phlogopites. *Science* 289:609–11

Ketcham RA. 1996. Thermal models of core-complex evolution in Arizona and New Guinea: implications for ancient cooling paths and present-day heat flow. *Tectonics* 15:933–51

Ketcham RA. 2005. Forward and inverse modeling of low-temperature thermochronometry data. See Reiners & Ehlers 2005, 58:275–314

Ketcham RA, Donelick RA, Carlson WD. 1999. Variability of apatite fission-track annealing kinetics. III. Extrapolation to geological time scales. *Am. Mineral.* 84:1235–55

Kirchner JF, Finkel RC, Riebe CS, Granger DE, Clayton JL, et al. 2001. Mountain erosion over 10 yr, 10 k.y., and 10 m.y. time scales. *Geology* 29:591–94

Kramar N, Cosca MA, Hunziker JC. 2001. Heterogeneous $^{40}Ar^{*}$ distributions in naturally deformed muscovite: in situ UV-laser ablation evidence for microstructurally controlled intragrain diffusion. *Earth Planet Sci. Lett.* 192:377–88

Kohn BP, Belton DX, Brown RW, Gleadow AJW, Green PF, Lovering JF. 2003. Comment on: "Experimental evidence for the pressure dependence of fission track annealing in apatite" by A.S. Wendt et al. [Earth Planet. Sci. Lett. 201 2002 593–607]. *Earth Planet. Sci. Lett.* 215:299–306

Koons PO, Norris RJ, Craw D, Cooper AF. 2003. Influence of exhumation on the structural evolution of transpressional plate boundaries: an example from the Southern Alps, New Zealand. *Geology* 31:3–6

Koons PO, Zeitler PK, Chamberlain CP, Craw D, Meltzer AS. 2002. Mechanical links between erosion and metamorphism in Nanga Parbat, Pakistan Himalaya. *Am. J. Sci.* 302:749–73

Laslett GM, Green PF, Duddy IR, Gleadow AJW. 1987. Thermal annealing of fission tracks in apatite 2. A quantitative analysis. *Chem. Geol. (Isotope Geosci. Sect.)* 65:1–13

Lavé J, Avouac JP. 2001. Fluvial incision and tectonic uplift across the Himalayas of central Nepal. *J. Geophys. Res.* 106:26561–91

Lister GS, Baldwin SL. 1996. Modelling the effect of arbitrary P-T-t histories on argon diffusion in minerals using the MacArgon program for the Apple Macintosh. *Tectonophysics* 253:83–109

Mancktelow NS, Grasemann B. 1997. Time-dependent effects of heat advection and topography on cooling histories during erosion. *Tectonophysics* 270:167–95

McDougall I, Harrison TM. 1999. *Geochronology and Thermochronology by the $^{40}Ar/^{39}Ar$ Method*. Oxford: Oxford Univ. Press. 269 pp. 2nd ed.

Meesters AGCA, Dunai TJ. 2002. Solving the production-diffusion equation for finite diffusion domains of various shapes. Part I. Implications for low-temperature (U-Th)/He thermochronology. *Chem. Geol.* 186:333–44

Molnar P. 2004. Late Cenozoic increases in accumulation rates of terrestrial sediment: how might climate change have affected erosion rates? *Annu. Rev. Earth Planet. Sci.* 32:67–89

Molnar P, England P. 1990. Late Cenozoic uplift of mountain ranges and global climate change: chicken or egg? *Nature* 346:29–34

Montgomery DR. 2002. Valley formation by fluvial and glacial erosion. *Geology* 30:1047–50

Moore MA, England PC. 2001. On the inference of denudation rates from cooling ages of minerals. *Earth Planet. Sci. Lett.* 185:265–84

Mulch A, Cosca M, Handy M. 2002. In-situ UV-laser $^{40}Ar/^{39}Ar$ geochronology of a micaceous mylonite: an example of defect-enhanced argon loss. *Contrib. Mineral. Petrol.* 142:738–52

Naeser CW, Faul H. 1969. Fission track annealing in apatite and sphene. *J. Geophys. Res.* 74:705–710

Nasdala L, Wenzel M, Vavra G, Irmer G, Wenzel T, Bernd K. 2001. Metamictization of natural zircon: accumulated versus thermal annealing of radioactivity-induced damage. *Contrib. Mineral. Petrol.* 141:125–44

Parrish RR. 1983. Cenozoic thermal evolution and tectonics of the Coast Mountains of British Columbia 1. Fission-track dating, apparent uplift rates, and patterns of uplift. *Tectonics* 2:601–31

Pazzaglia FJ, Brandon MT. 1996. The macrogeomorphic evolution of the post-Triassic Appalachian Mountains determined by deconvolution of the offshore basin sedimentary record. *Basin Res.* 8:255–78

Pazzaglia FJ, Brandon MT. 2001. A fluvial record of long-term steady-state uplift and erosion across the Cascadia Forearc High, Western Washington State. *Am. J. Sci.* 301:385–431

Porter SC. 1981. Pleistocene glaciation in the southern Lake District of Chile. *Quat. Res.* 16:263–92

Rahl J, Reiners PW, Campbell IH, Nicolescu S, Allen CM. 2003. Combined single grain (U-Th)/He and U/Pb dating of detrital zircons from the Navajo Sandstone, Utah. *Geology* 31:761–64

Rahn MK, Brandon MT, Batt GE, Garver JI. 2004. A zero-damage model for fission-track annealing in zircon. *Am. Mineral.* 89:473–84

Reiners PW, Brady R, Farley KA, Fryxell JE, Wernicke B, Lux D. 2000. Helium and argon thermochronometry of the Gold Butte block, south Virgin Mountains, Nevada. *Earth Planet. Sci. Lett.* 178:315–26

Reiners PW, Campbell IH, Nicolescu S, Allen CM, Hourigan JK, et al. 2005a. (U-Th)/(He-Pb) double dating of detrital zircons. *Am. J. Sci.* 305:259–311

Reiners PW, Ehlers TA, eds. 2005. *Low-Temperature Thermochronology: Techniques, Interpretations, Applications. Reviews in Mineralogy and Geochemistry*, Vol. 58. Chantilly, VA: Mineral. Soc. Am., Geochem. Soc. 622pp.

Reiners PW, Ehlers TA, Mitchell SG, Montgomery DR. 2003a. Coupled spatial variations in precipitation and long-term erosion rates across the Washington Cascades. *Nature* 426:645–47

Reiners PW, Ehlers TA, Zeitler PK. 2005b. Past, present, and future of thermochronology. In See Reiners & Ehlers 2005, 58:1–18

Reiners PW, Farley KA. 1999. Helium diffusion and (U-Th)/ He thermochronometry of titanite. *Geochim. Cosmochim. Acta* 63:3845–59

Reiners PW, Farley KA. 2001. Influence of crystal size on apatite (U-Th)/He thermochronology: an example from the Bighorn Mountains, Wyoming. *Earth Planet. Sci. Lett.* 188:413–20

Reiners PW, Spell TL, Nicolescu S, Zanetti KA. 2004. Zircon (U-Th)/He thermochronometry: He diffusion and comparisons with $^{40}Ar/^{39}Ar$ dating. *Geochim. Cosmochim. Acta* 68:1857–87

Reiners PW, Zhou Z, Ehlers TA, Xu C, Brandon MT, et al. 2003b. Post-orogenic evolution of the Dabie Shan, eastern China, from (U-Th)/He and fission-track dating. *Am. J. Sci.* 303:489–518

Riebe CS, Kirchner JW, Finkel RC. 2003. Long-term rates of weathering and physical erosion from cosmogenic nuclides and geochemical mass balance. *Geochim. Cosmochim. Acta* 67:4411–27

Ring U, Brandon MT, Willett SD, Lister GS. 1999a. Exhumation processes. See Ring et al. 1999b, 154:1–27

Ring U, Brandon MT, Lister GS, Willett SD, eds. 1999b. *Exhumation Processes: Normal Faulting, Ductile Flow, and Erosion*. London: Geol. Soc. Lond. Spec. Pub.

Robbins GA. 1972. *Radiogenic argon diffusion in muscovite under hydrothermal conditions*. MS thesis. Brown Univ., Providence, RI

Royden L. 1996. Coupling and decoupling of crust and mantle in convergent orogens: implications for strain partitioning in the crust. *J. Geophys. Res.* 101:17679–705

Ruhl KW, Hodges KV. 2005. The use of detrital mineral cooling ages to evaluate steady-state assumptions in active orogens: an example from the central Nepalese Himalaya. *Tectonics*. 24:TC4015, doi:10.1029/2004TC001712

Scott RJ, Foster DA, Lister GS. 1998. Tectonic implications of rapid cooling of lower plate rocks from the Bucksin-Rawhide metamorphic core complex, west-central Arizona. *Geol. Soc. Am. Bull.* 110:588–614

Sherlock SC. 2001. Two-stage erosion and deposition in a continental margin setting; an $^{40}Ar/^{39}Ar$ laserprobe study of offshore detrital white micas in the Norwegian Sea. *J. Geol. Soc. Lond.* 158(Pt. 5):793–99

Shuster DL, Farley KA. 2003. $^{4}He/^{3}He$ thermochronometry. *Earth Planet. Sci. Lett.* 217:1–17

Shuster DL, Farley KA. 2005. $^{4}He/^{3}He$ thermochronometry. See Reiners & Ehlers 2005, 58:181–203

Shuster DL, Ehlers TA, Rusmore ME, Farley KA. 2005. Rapid glacial erosion at 1.8 Ma revealed by $^{4}He/^{3}He$ thermochronometry. *Science* 310:1668–70

Shuster DL, Farley KA, Sisterson JM, Burnett DS. 2003. Quantifying the diffusion kinetics and spatial distributions of radiogenic ^{4}He in minerals containing proton-induced ^{3}He. *Earth Planet. Sci. Lett.* 217:19–32

Simpson G. 2004. Role of river incision in enhancing deformation. *Geology* 32:341–44

Small EE, Anderson RS. 1998. Pleistocene relief production in Laramide mountain ranges, western United States. *Geology* 26:123–26

Spotila JA, Buscher JT, Meigs AJ, Reiners PW. 2004. Long-term glacial erosion of active mountain belts: example of the Chugach–St. Elias Range, Alaska. *Geology* 32:501–4

Spotila JA, Farley K, Yule JD, Reiners PW. 2001. Near-field transpressive deformation along the San Andreas fault zone in southern California, based on exhumation constrained by (U-Th)/He dating. *J. Geophys. Res.* 106:30909–29

Stewart RJ, Brandon MT. 2004. Detrital zircon fission-track ages for the "Hoh Formation": implications for late Cenozoic evolution of the Cascadia subduction wedge. *Geol. Soc. Am. Bull.* 116:60–75

Stock JD, Montgomery DR. 1996. Estimating palaeorelief from detrital mineral age ranges. *Basin Res.* 8:317–27

Stockli DF. 2005. Application of low-temperature thermochronometry to extensional tectonic settings. See Reiners & Ehlers 2005, 58:411–448

Stockli DF, Farley KA. 2004. Empirical constraints on the titanite (U–Th)/He partial retention zone from the KTB drill hole. *Chem. Geol.* 227:223–36

Stockli DF, Farley KA, Dumitru TA. 2000. Calibration of the apatite (U-Th)/He thermochronometer on an exhumed fault block, White Mountains, California. *Geology* 28:983–86

Stuewe K, White L, Brown R. 1994. The influence of eroding topography on steady-state isotherms: application to fission track analysis. *Earth Planet. Sci. Lett.* 124:63–74

Tagami T, Galbraith RF, Yamada R, Laslett GM. 1998. Revised annealing kinetics of fission tracks in zircon and geologic implications. In *Advances in Fission-Track Geochronology*, ed. P van den Haute, F De Corte, pp. 99–112. Dordrecht: Kluwer Acad. Publ.

Tagami T, Ito H, Nishimura S. 1990. Thermal annealing characteristics of spontaneous fission tracks in zircon. *Chem. Geol. (Isotope Geosci. Sec.)* 80:159–69
Tomkin JH, Braun J. 2002. The influence of alpine glaciation on the relief of tectonically active mountain belts. *Am. J. Sci.* 302:169–90
Vai GB, Martini IP. 2001. *Anatomy of an Orogen: The Apennines and Adjacent Mediterranean Basins*. Dordrecht: Kluwer Acad. Publ. 656pp.
Wagner GA, Reimer GM. 1972. Fission track tectonics: the tectonic interpretation of fission track ages. *Earth Planet. Sci. Lett.* 14:263–68
Wagner GA, Reimer GM, Jäger E. 1977. Cooling ages derived by apatite fission track, mica Rb-Sr, and K-Ar dating: the uplift and cooling history of the central Alps. *Mem. Inst. Geol. Mineral. Univ. Padova* 30:1–27
Wagner GA, van den Haute P. 1992. *Fission-Track Dating*. Dordrecht: Kluwer Acad. Publ. 285pp.
Weiland RJ, Cloos M. 1996. Pliocene-Pleistocene asymmetric unroofing of the Irian fold belt, Irian Jaya, Indonesia: apatite fission-track thermochronology. *Geol. Soc. Am. Bull.* 108:1438–49
Wendt AS, Vidal O, Chadderton LT. 2002. Experimental evidence for the pressure dependence of fission track annealing in apatite. *Earth Planet. Sci. Lett.* 201:593–607
Whipple K, Kirby E, Brocklehurst S. 1999. Geomorphic limits to climatically induced increases in topographic relief. *Nature* 401:39–43
Whipple KX, Meade BJ. 2004. Controls on the strength of coupling among climate, erosion, and deformation in two-sided, frictional orogenic wedges at steady state. *J. Geophys. Res.* 109: F01011, doi:10.1029/2003JF000019
White NM, Pringle M, Garzanti E, Bickle M, Najman Y, et al. 2002. Constraints on the exhumation and erosion of the High Himalayan Slab, NW India, from foreland basin deposits. *Earth Planet. Sci. Lett.* 195:29–44
Willett SD. 1999. Orogeny and orography: the effects of erosion on the structure of mountain belts. *J. Geophys. Res.* 104:28957–81
Willett S, Beaumont C. 1994. Insights into the tectonics of the India-Asia collision from numerical models of mantle subduction. *Nature* 369:642–45
Willett S, Beaumont C, Fullsack P. 1993. Mechanical models for the tectonics of doubly vergent compressional orogens. *Geology* 21:371–74
Willett SD, Brandon MT. 2002. On steady states in mountain belts. *Geology* 30:175–78
Wobus CW, Heimsath A, Whipple K, Hodges K. 2005. Out-of-sequence thrust faulting in the central Nepalese Himalaya. *Nature* 434:1008–11
Wobus CW, Hodges KV, Whipple KX. 2003. Has focused denudation sustained active thrusting at the Himalayan topographic front? *Geology* 31:861–64
Wolf RA, Farley KA, Kass DM. 1998. Modeling of the temperature sensitivity of the apatite (U-Th)/ He thermochronometer. *Chem. Geol.* 148:105–14
Yamada R, Tagami T, Nishimura S, Ito H. 1995. Annealing kinetics of fission tracks in zircon: an experimental study. *Chem. Geol. (Isotope Geosci. Sec.)* 122:249–58
Yamada K, Tagami T, Shimobayashi N. 2003. Experimental study on hydrothermal annealing of fission tracks in zircon. *Chem. Geol.* 201:351–57

Zattin M, Picotti V, Zuffa GG. 2002. Fission-track reconstruction of the front of the Northern Appenines thrust wedge and overlying Ligurian unit. *Am. J. Sci.* 302:346–79

Zaun PE, Wagner GA. 1985. Fission-track stability in zircons under geological conditions. *Nucl. Tracks Radiation Meas.* 10:303–7

Zeitler PK, Herczeg AL, McDougall I, Honda M. 1987. U-Th-He dating of apatite: a potential thermochronometer. *Geochim. Cosmochim. Acta* 51:2865–68

Zeitler PK, Meltzer AS, Koons PO, Craw D, Hallet B, et al. 2001. Erosion, Himalayan geodynamics, and the geomorphology of metamorphism. *GSA Today* 11:4–9

Errata for:

Reiners, P. W., and Brandon Mark, T., 2006, Using thermochronology to understand orogenic erosion: Annual Review of Earth and Planetary Sciences, v. 34, p. 419–66, doi: 10.1146/annurev.earth.34.031405.125202.

1) The number 1 is missing from the denominator with the exponential expression in equation 8a. The correct equation is:

$$T(z) = T_S + \left(T_L\text{-}T_S + \frac{H_T L}{\dot{\varepsilon}} \right) \frac{1 - \exp\left(-\dot{\varepsilon}\, z/\kappa\right)}{1 - \exp\left(-\dot{\varepsilon}\, L/\kappa\right)} - \frac{H_T z}{\dot{\varepsilon}}, \qquad (8a)$$

2) The temperatures for the PRZ temperatures for the He and Ar systems shown in Figures 1a and 1c were incorrectly calculated due to a numerical error in the CLOSURE program. The temperatures were systematically too low by about 25°C. Corrected versions of these figures are included here. A corrected version of the CLOSURE program is available at www.geology.yale.edu/~brandon.

Note that these errors do not change any of the discussion or conclusions of our paper.

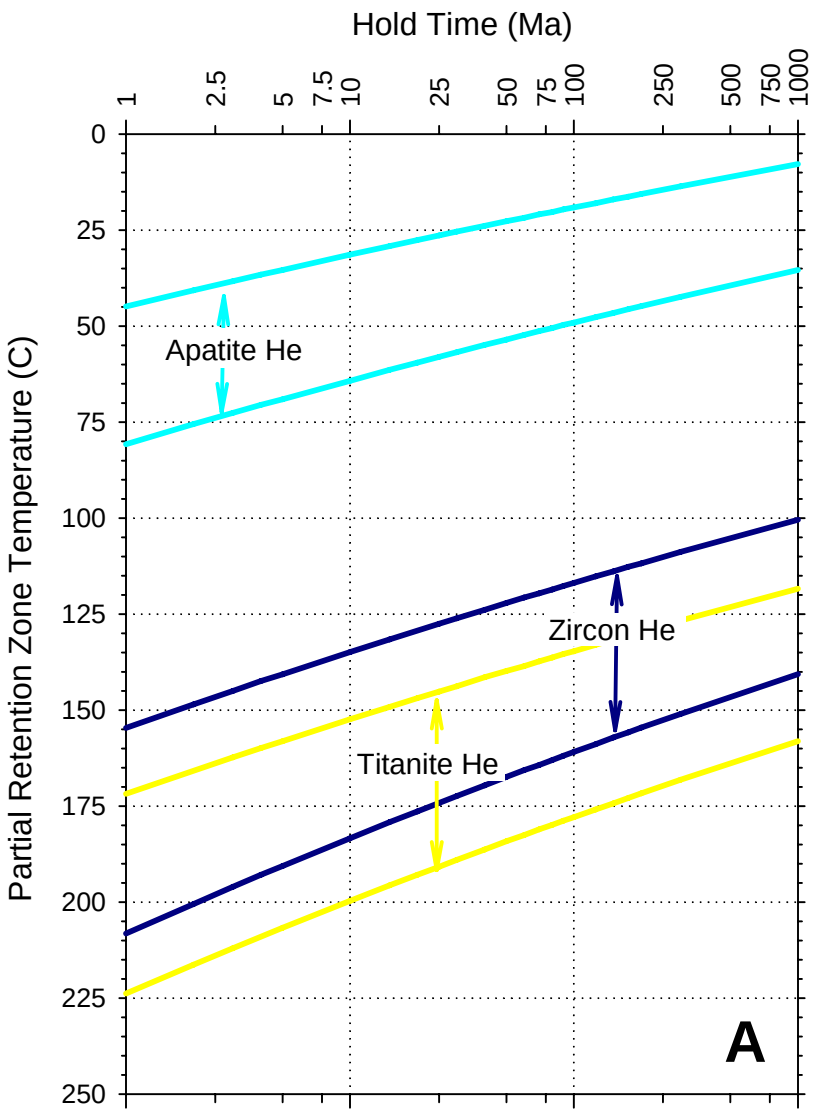

Reiners and Brandon (2006)
Figure 1a. Loss-only PRZ for He dating calculated using CLOSURE (corrected, June 24, 2007)

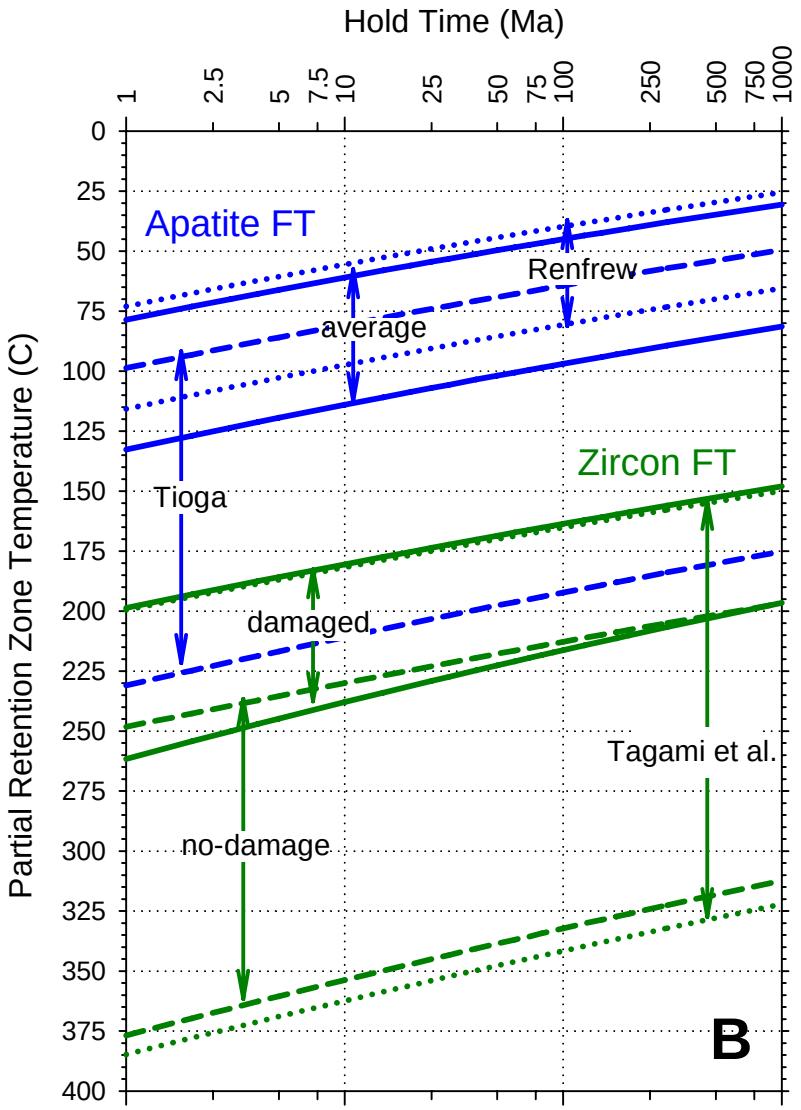

Reiners and Brandon (2006)
Figure 1b. Loss-only PRZ for FT dating calculated using CLOSURE (original published version was correct; included here for completeness).

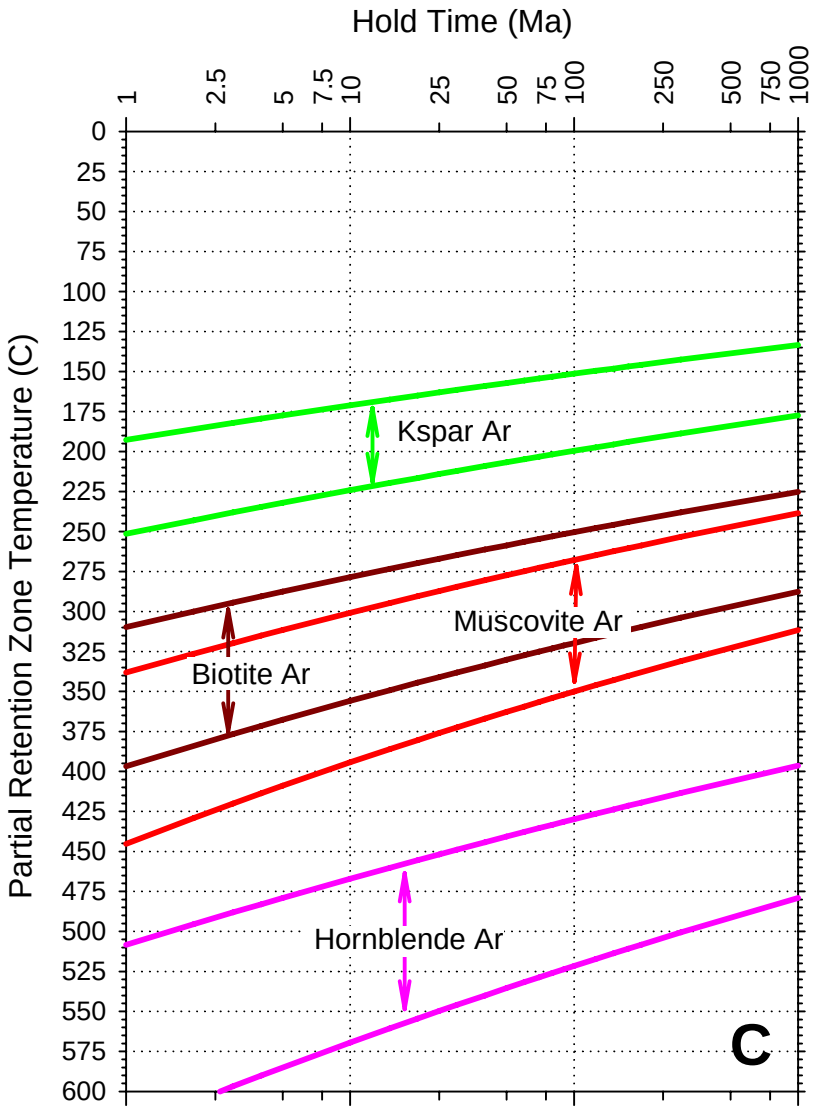

Reiners and Brandon (2006)
Figure 1c. Loss-only PRZ for Ar dating calculated using CLOSURE (corrected, June 24, 2007)